EUROPEAN COMMISSION

Community Research

RAPHAEL

Contract Number: 516508 (FI6O)

DELIVERABLE (D-FT2.1)

Author(s): **J.M.ESCLEINE**

Reporting period: e.g.
Date of issue of this report :

Start date of project : **15/04/2005** Duration : **48 Months**

Project co-funded by the European Commission under the Euratom Research and Training Programme on Nuclear Energy within the Sixth Framework Programme (2002-2006)		
Dissemination Level		
PU	Public	
RE	Restricted to the partners of the RAPHAEL project	
CO	Confidential, only for specific distribution list defined on this document	**X**

Distribution list

Person and organisation name and/or group	Comments
See the distribution list in the document	To comply with CEA QA

ReActor for Process heat, Hydrogen And ELectricity generation (RAPHAEL)		
Sub-project: SP-FT **Work package:** 2	**RAPHAEL document no:** RAPHAEL-0611-D-FT2-1	**Document type:** Deliverable
Issued by: CEA **Internal no.:** SESC/LLCC 06-014		**Document status:** Draft

Document title
DEFINITION OF THE PYCASSO IRRADIATION EXPERIMENT IN THE HFR (PETTEN) PRACTICALLY UNRESTRAINED DENSIFICATION OF SPHERICAL PYC LAYERS

Executive summary

This document theoretically and experimentally defines the part of the PYCASSO irradiation experiment dedicated to acquiring knowledge on the densification kinetics of pyrocarbon (OPyC) layers of particles from very recent fuel fabrication operations. On the grounds of microstructural representativeness, the spherical geometry was preferred to all other possible geometries. Emphasis is also placed on the statistical aspect of this experimental approach.

Revisions

Rev.	Date	Short description	Author	WP Leader	SP Leader	Coordinator
00		First issue	J.M. ESCLEINE CEA	K.BAKKER NRG	M.PHÉLIP CEA	E. BOGUSH FANP
01						

Direction de l'énergie nucléaire
Département d'études des combustibles
Service d'études et de simulation du comportement des combustibles

DEC

CADARACHE

DEFINITION OF THE PYCASSO IRRADIATION EXPERIMENT IN THE HFR (PETTEN)

PRACTICALLY UNRESTRAINED DENSIFICATION OF SPHERICAL PYC LAYERS

J.M.Escleine

Technical Note SESC/LLCC 06-014 – Index 0 – Septembre 2006

Commissariat à l'énergie atomique
Centre de Cadarache
DEN/CAD/DEC/SESC/LLCC - Bât 130 - 13108 SAINT-PAUL-LEZ-DURANCE CEDEX
Tel.: 04.42.25.32.01- Fax: 04.42.25.32.85 – E-Mail: llcclipa@drncad.cea.fr

Direction de l'énergie nucléaire
Département d'études des combustibles
Service d'études et de simulation du comportement des combustibles
Laboratoire des lois de comportement du combustible

DEFINITION OF THE PYCASSO IRRADIATION EXPERIMENT IN THE HFR (PETTEN) PRACTICALLY UNRESTRAINED DENSIFICATION OF SPHERICAL PYC LAYERS

Author(s)	**J.M.Escleine**		
Reference	**Technical note SESC/LLCC 06-014 – Ind. 0**		
Scope	DDIN/DPSF/CCC		
Classification	Free		
EOTP No.	A-CDHTR-06-01	Number of pages:	55

Reference and date of initial release:

Abstract:

This document theoretically and experimentally defines the part of the PYCASSO irradiation experiment dedicated to acquiring knowledge on the densification kinetics of pyrocarbon (OPyC) layers of particles from very recent fuel fabrication operations.

On the grounds of microstructural representativeness, the spherical geometry was preferred to all other possible geometries.

Emphasis is also placed on the statistical aspect of this experimental approach.

	WRITTEN BY	CHECKED BY	APPROVED BY	ISSUED BY
NAME	J.M.ESCLEINE	M. PHÉLIP	C. VALOT	L. BRUNEL
SIGNATURE				

AFAQ ISO 9001 VERSION 2000
DEC

DISTRIBUTION LIST

EXTERNAL DISTRIBUTION

COMPANY	NAME	NUMBER OF COPIES	COMMENTS

INTERNAL DISTRIBUTION

Dpt/Service/Lab	NAME	NUMBER OF COPIES	COMMENTS

REVIEW

DATE	OBJECT OF REVIEW	INDEX
SEPTEMBRE 2006	FIRST DRAFT	0

TABLE OF CONTENTS

1. CONTEXT AND GENERAL OBJECTIVES **9**

2. CHOICE OF SPHERICAL GEOMETRY **10**

2.1. PLANE GEOMETRY 10

2.2. SPHERICAL GEOMETRY 13

3. ANALYTICAL MECHANICAL APPROACH FOR THE BISO FUEL PARTICLE **14**

3.1. GENERAL CASE 14

3.2. SPECIFIC CASES WHERE f_K DOES NOT DEPEND ON THE RADIUS 18

3.3. COMPARISON WITH THE ATLAS CODE 20

4. POTENTIAL OF EXPERIMENTAL EVALUATIONS ON BISO **22**

4.1. PARAMETERS $\eta_{//}$ & $\eta_{\perp}$ 22

4.2. PARAMETERS K AND ν 24

5. IRRADIATION EXPERIMENT OPTIONS **26**

5.1. BUFFER SHRINKAGE POTENTIAL 28

5.2. PARTICLE TYPES 31

6. ASSESSMENT AND EVOLUTION OF UNCERTAINTIES **31**

6.1. RADIUS AND THICKNESS MEASUREMENTS 32

6.2. RADIUS AND DENSIMETRIC MEASUREMENTS OF THE OPYC LAYER 32

6.3. NUMERICAL APPLICATIONS 33

6.4. EFFECT OF VARIATION IN X 33

6.5. PROPOSAL OF A DIMENSIONAL MEASUREMENT METHOD 34

7. STATISTICAL ASPECTS **35**

8. DRUM COMPOSITION **35**

9. CHARACTERISATION AND POST-IRRADIATION EXAMINATIONS **39**

10. IRRADIATION PARAMETERS **40**

11. CONCLUSION **40**

REFERENCES **42**

FIGURES **44**

1. CONTEXT AND GENERAL OBJECTIVES

This document focuses on the part of the PYCASSO* experiment dealing with the densification of pyrocarbon under irradiation in the high flux reactor (HFR) in Petten. The PYCASSO experiment is part of R&D on very high temperature reactors (VHTR), one of the six nuclear reactor concepts meeting criteria in terms of safety, sustainable development, non-proliferation and fuel-efficiency as identified in the Generation IV initiative.

This irradiation experiment is carried out under the aegis of the RAPHAEL† project. The CEA is in charge of defining the experimental irradiation conditions, the geometry and the number of samples to be irradiated, as well as fabricating these samples. The Nuclear Research Consultancy Group (NRG) is in charge of designing the sample holder and the device, as well as its irradiation.

As part of the Generation IV initiative, the programme also involves various partners and particularly the Americans, who will irradiate the creep specimens. This topic will not be discussed in this paper.

In relation to past fuel particle fabrications, the PYCASSO experiment mainly aims to acquire knowledge on **densification kinetics under conditions in which the pyrocarbon layers composed of new fuel particles are free of any significant stress**. The main priority therefore involves determining the tangential and radial strain in the PyC layers in relation to the fast flux owing to dimensional changes caused by neutron irradiation (source terms).

The statistical aspect of the experimental approach (global approach) is also highlighted in this paper.

* **PY**rocarbon Irradiation for **C**reep **A**nd **S**welling/**S**hrinkage of **O**bjects
† **R**e**A**ctor for **P**rocess heat, **H**ydrogen **A**nd **EL**ectricity generation

2. CHOICE OF SPHERICAL GEOMETRY

2.1. PLANE GEOMETRY

Most data on dimensional changes due to the neutron irradiation of pyrocarbon layers (IPyC and OPyC) result from dimensional and densimetric measurements performed on small strips taken from deposits obtained by introducing dedicated particles of small, flat substrates into a fluid bed. These are more than often graphite disks such as the one illustrated below (diagram from Reference [1]):

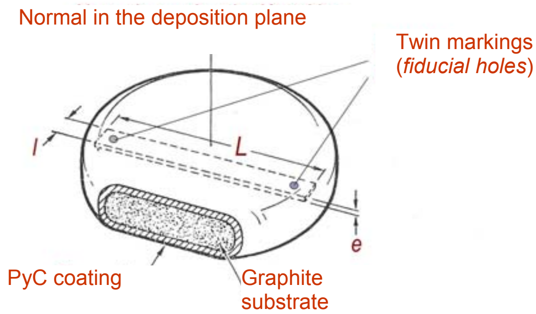

Such disks are considered as being potentially much easier and more flexible to use under experimental conditions (particularly BAF‡ measurements) than deposits on spheres. Deposits thus obtained are either stripped of their substrate to be irradiated unrestrained, or are irradiated restrained on an unyielding support. The approximate size of characteristic strips is 6 mm long (*L*) by 300 µm to 1 mm wide (ℓ) and 25 to 100 µm thick (*e*); the disk itself is about one millimetre thick.

Dimensional changes parallel to the deposition plane are estimated based on the variation in the distance between two holes drilled through the sample (a diameter of about 150 µm).

The accuracy of dimensional measurements is generally about one micron, whereas the accuracy of densimetric (flotation) measurements is generally better than 0.03% (up to ± 0.0001).

2.1.1. Determining parameters $\eta_{//}$, $\eta_{\perp}$, *K* and ν

Except for specific cases, definitions of quantities are provided in § 3.

On the condition that geometric changes are homogeneous, particularly in terms of thicknesses, the conservation of mass and various geometric considerations make it possible to write the following expression *[2]* :

$$\ln(1+\Delta d/d)+2\ln(1+\Delta L/L)+\ln(1+\Delta e/e)=0$$

‡ *Bacon Anisotropy Factor*

Let:

$$\ln\left(1+\Delta d/d\right)+2\,\varepsilon_{//}+\varepsilon_{\perp}=0 \qquad (1)$$

where $\Delta L/L$ (= $\Delta \ell / \ell$) represents the relative change in the length between holes.

In the case of strictly unrestrained strain, the relationship (1) is written as follows:

$$\ln\left(1+\Delta d/d\right)+2\,\eta_{//}+\eta_{\perp}=0 \qquad (2)$$

Experimentally obtaining the entity $\eta_{//}$ directly results from the measurement of ΔL, with $\eta_{\perp}$ being inferred from (2) by determining Δd —, which is much more accurate than that of Δe.

<u>Comment</u>: According to [3][4], the change in density can be explained by the accommodation of crystallite dimensional changes by the pores of different natures, which is assumed to significantly and isotropically contribute to the overall dimensional change, adding the term $-\frac{1}{3}\ln\left(1+\Delta d/d\right)$ *to each strain resulting from the reorganisation of the crystallites. The rearrangement of the crystallites is assumed to be anisotropic, yet mainly isochoric in the initial phase*.

The simultaneous irradiation of unrestrained and restrained strips on their support potentially provides access to ν, and then K — based on the hypothesis of isotropic creep. In this case, the irradiation creep strain $\varepsilon_{c//}$ and $\varepsilon_{c\perp}$ are expressed by the following relationship (elastic strains are considered negligible and $\sigma_{\perp}$ non-existent):

$$\varepsilon_{c\perp}=\left(\Delta e/e\right)_{rest.}-\left(\Delta e/e\right)_{lib.}=-\int_0^{\gamma_0}2K\,\nu\,\sigma_{//}\,d\gamma \qquad (3)$$

$$\varepsilon_{c//}=\left(\Delta L/L\right)_{rest.}-\left(\Delta L/L\right)_{lib.}=\int_0^{\gamma_0}K\left(1-\nu\right)\sigma_{//}\,d\gamma \qquad (4)$$

Insofar as it is accepted as a first-order approximation that the two creep parameters are independent of the fluence γ *[5]* (i.e.: microstructural changes), the following relationships are obtained by dividing (3) by (4):

$$\left(\varepsilon_{c\perp}/\varepsilon_{c//}\right)=-2\nu/\left(1-\nu\right) \qquad (5)$$

that is:

$$\nu=\left(\varepsilon_{c\perp}/\varepsilon_{c//}\right)/\left\{\left(\varepsilon_{c\perp}/\varepsilon_{c//}\right)-2\right\} \qquad (6)$$

According to *[5]*, ν comes close to 0.5 (constant volume) with low strains before rapidly decreasing and stabilising around 0.4 regardless of the structure, density or temperature. Irradiations in a restrained configuration led to a reduction in the intensity of PyC densification in comparison to irradiations in an unrestrained configuration, which is coherent with a ν coefficient less than 0.5. Determining *K* is a more complicated matter.

Prior knowledge of changes in $\eta_{//}$ and $\eta_{\perp}$ as a function of the fluence and ν, as well as knowledge of the Young modulus and Poisson's ratio theoretically makes it possible to deduce *K* from the formalism obtained from the analytical treatment of the mechanics of a restrained strip (systematically under biaxial traction). Complications arise from the fact that, strictly speaking, the entities $\eta'_{//}$ and $\eta'_{\perp}$ depend on the degree of anisotropy and therefore the change in the state of stress (see § 4.1). In other words and assuming that the parameter *K* is not sensitive to changes in the degree of anisotropy, it is **strictly speaking** necessary to have entities $\eta'_{//}$ and $\eta'_{\perp}$ that take into account this change. For this reason, the experimentally-complex procedure (to be repeated as many times as necessary) involves:

- Characterising (geometry, density and quantification of anisotropy) and irradiating a homogeneous group of geometrically-restrained samples for a given time,

- Characterising this group once again, taking note that it is impossible to control the intensity and change in the stress (seeing it is self-generated), which results in a new state of anisotropy,

- Resuming unrestrained irradiation (normal procedure) of the entire group (case of non-destructive testing) or part of the group – not concerned by non-destructive testing (possibly destructive testing in this case).

Ultimately, changes in relation to the fluence of $\eta'_{//}$ and $\eta'_{\perp}$ are obtained taking into account – all things considered – changes in the anisotropic level of PyC; this makes it possible to calculate the coefficient K.

2.1.2. Microstructural representativeness of deposits

It is more or less implicitly and consensually agreed by experimenters that if disk coatings display the same density and anisotropy, as well as being carried out at the same deposit speed as coatings on particles, they will therefore share the same properties and behave in the same way [6].

It nevertheless seems practically impossible to reproduce the microstructure of a spherical particle coating on a plane support simultaneously in the same fluid bed, i.e.: **under the same deposit conditions** (temperature, pressure, gas composition, transport kinetics of molecules to the substrate, etc.), particularly owing to the fact that on a plane support:

- The deposit thickness is not constant (orientation in relation to the gaseous flux),

- The surface-volume ratio is very different to that of a coated particle,
- The residual stresses act differently,

and the disks do not circulate in the same manner as the spheres within the fluid bed.

Inasmuch as the parameters for comparison have been completely identified, obtaining an identical microstructure requires determining the suitable (and therefore different) deposit conditions, which in turn engenders a lot of trial and error to be managed in terms of physical measurements and inevitably generates a certain amount of approximation. In any case, measurements will notably reflect the imperfections (cracks, pores, composition heterogeneities, etc.) inherent to deposits on plane supports. Another problem is the evaluation of consequences of the physical separation the strips from their supports.

2.2. SPHERICAL GEOMETRY

Even if the homology of the microstructure remains to be checked in relation to the mean diameter of the PyC layer, this geometry intrinsically seems to be the most appropriate for reproducing the behaviour of PyC and SiC of standard fuel particles.

In this geometry, the technique that most resembles what is currently used on plane samples involves the unrestrained irradiation of the PyC strips or fragments – rather than rings to encourage the relaxation of residual stress – debonded from initially complete particles. The same types of measurements and processing as those used on rectilinear strips are therefore accessible but must take into account the radius of curvature *[7]* when dealing with lengths.

According to Reference *[7]*, it is generally possible to obtain equivalent processing methods to those used for rectilinear strips when comparing unrestrained changes with restrained changes in SiC deposits (OPyC) under the same irradiation conditions by assimilating the deposit to a thin shell and by ignoring geometric changes in SiC – a similar approach to that consisting in depositing PyC directly in contact with a kernel of corundum (sapphire) *[8]* .

The relevance of this experimental approach lies in the knowledge that the correct PyC microstructure is being tested – at least in terms of the “fuel diameter” – not to mention that it is possible to produce a great number of samples that are, in principle, identical (statistics) before irradiating them in a minimum amount of space. However, the extreme care required when using this technique seems contradictory with the intention of using a statistical approach. Moreover and without going into details, this technique designed to obtain identical data to those accessible in a plane geometry actually renders the procedures even more cumbersome and rules out the use of any statistical approach; this is confirmed by the fact that to our knowledge, the literature does not mention any such use.

The homology of the microstructure raises the question as to how the spherical geometry could possibly contribute to data on PyC behaviour in a context preferring global statistical treatment and the "maximum simplification" of experimental and fabrication procedures, even if this requires both rather substantial modelling efforts for result interpretation and experimental compromise in terms of irradiation preparation and measurements.

Such concerns resulted in the development of a global BISO fuel particle approach with an inert kernel for which the theoretical and experimental aspects will be described in this document.

3. ANALYTICAL MECHANICAL APPROACH FOR THE BISO FUEL PARTICLE

3.1. GENERAL CASE

The mechanical analysis below describes the spatial and temporal change (fluence) in strain and stress generated in the **outer layer of a BISO particle** (kernel/buffer/PyC), i.e.: the OPyC layer. This analysis resumes the analysis developed by J.L. KAAE *[Erreur ! Signet non défini.]*.

The following basic expressions are **compatibility equations** expressed as spherical coordinates (without shear):

$$\varepsilon_{//} = \frac{u}{r} \tag{7}$$

$$\varepsilon_{\perp} = \frac{du}{dr} \tag{8}$$

where $\varepsilon_{//}$ represents the total tangential (or orthoradial) strain, $\varepsilon_{\perp}$ represents the total radial strain and u is the radial displacement of the radius r,

and the **balance equation**:

$$\frac{d\sigma_{\perp}}{dr} + \frac{2}{r}\left(\sigma_{\perp} - \sigma_{//}\right) = 0 \tag{9}$$

where $\sigma_{//}$ and $\sigma_{\perp}$ represent stresses in the tangential and radial directions respectively.

Total strains can be expressed as follows:

$$\varepsilon_{//} = \varepsilon_{e//} + \varepsilon_{c//} + \eta_{//} \tag{10}$$

$$\varepsilon_{\perp} = \varepsilon_{e\perp} + \varepsilon_{c\perp} + \eta_{\perp} \tag{11}$$

where $\varepsilon_{e//}$ and $\varepsilon_{e\perp}$ represent elastic strains in the tangential and radial directions, $\varepsilon_{c//}$ and $\varepsilon_{c\perp}$ represent homologous strains resulting from irradiation creep, and $\eta_{//}$ and $\eta_{\perp}$ represent homologous strains caused by PyC dimensional changes owing to neutron irradiation (source terms).

Thermal creep is ignored as it is considered negligible in relation to the temperatures in question, nor is thermal expansion taken into account, assumed to be isotropic and not generating stress.

When Young's modulus E and Poisson's ratio μ depend on the fast neutron fluence, the elastic strains are expressed as follows:

$$\varepsilon_{e\perp} = \int_0^{\gamma_0} \frac{1}{E} \sigma'_{\perp}\, d\gamma - \int_0^{\gamma_0} \frac{2\mu}{E} \sigma'_{//}\, d\gamma \tag{12}$$

$$\varepsilon_{e//} = \int_0^{\gamma_0} \frac{1-\mu}{E} \sigma'_{//}\, d\gamma - \int_0^{\gamma_0} \frac{\mu}{E} \sigma'_{\perp}\, d\gamma \tag{13}$$

where the symbol "prim" indicates the derivation in relation to the fast fluence γ and γ_0 represents the fluence value according to which stress and strain are assessed.

Based on the assumption that stationary irradiation creep (excluding primary creep) experimentally validated for polycrystalline graphite (uniaxial behaviour) [9] can be generalised to cover PyC subject to a multiaxial state of stress, the following equations are obtained:

$$\dot{\varepsilon}_{c1} = K\left[\sigma_1 - \nu \cdot (\sigma_2 + \sigma_3)\right]\dot{\gamma}$$

$$\dot{\varepsilon}_{c2} = K\left[\sigma_2 - \nu \cdot (\sigma_1 + \sigma_3)\right]\dot{\gamma}$$

$$\dot{\varepsilon}_{c3} = K\left[\sigma_3 - \nu \cdot (\sigma_1 + \sigma_2)\right]\dot{\gamma}$$

where $\dot{\varepsilon}_{c1}$, $\dot{\varepsilon}_{c2}$ and $\dot{\varepsilon}_{c3}$ represent the stationary creep rates in the three main directions, σ_1, σ_2 and σ_3 represent the three main stress, whereas K and ν are respectively coefficients (considered isotropic) for irradiation creep and "Poisson's ratio in terms of stationary irradiation creep" [5].

In this case, the following expression applies:

$$\varepsilon_{c\perp} = \int_0^{\gamma_0} K\,\sigma_{\perp}\, d\gamma - \int_0^{\gamma_0} 2K\nu\,\sigma_{//}\, d\gamma \tag{14}$$

$$\varepsilon_{c//} = \int_0^{\gamma_0} K(1-\nu)\sigma_{//}\, d\gamma - \int_0^{\gamma_0} K\nu\,\sigma_{\perp}\, d\gamma \tag{15}$$

The equations (10) and (11) are therefore expressed as follows:

$$\varepsilon_{//} = \int_0^{\gamma_0} \left[\frac{1-\mu}{E}\sigma'_{//} - \frac{\mu}{E}\sigma'_{\perp} + K(1-\nu)\sigma_{//} - K\nu\sigma_{\perp} \right] d\gamma + \eta_{//} \tag{16}$$

$$\varepsilon_{\perp} = \int_0^{\gamma_0} \left[-\frac{2\mu}{E}\sigma'_{//} + \frac{1}{E}\sigma'_{\perp} - 2K\nu\sigma_{//} + K\sigma_{\perp} \right] d\gamma + \eta_{\perp} \tag{17}$$

By differentiating (7) in relation to *r*, the following is obtained:

$$\frac{du}{dr} = r\frac{d\varepsilon_{//}}{dr} + \frac{u}{r}$$

By substituting (7) and (8), the following is obtained:

$$\varepsilon_{\perp} = r\frac{d\varepsilon_{//}}{dr} + \varepsilon_{//}$$

or by differentiating in relation to γ:

$$\varepsilon'_{\perp} = r\frac{d\varepsilon'_{//}}{dr} + \varepsilon'_{//}$$

Based on (16) and (17), and by grouping the terms, the following equation is established:

$$\begin{aligned} & r\frac{(1-\mu)}{E}\frac{d\sigma'_{//}}{dr} - \frac{\mu}{E}r\frac{d\sigma'_{\perp}}{dr} + K(1-\nu)r\frac{d\sigma_{//}}{dr} - K\nu r\frac{d\sigma_{\perp}}{dr} \\ & + r\frac{d\eta'_{//}}{dr} + \frac{(1+\mu)}{E}\sigma'_{//} - \frac{(1+\mu)}{E}\sigma'_{\perp} + K(1+\nu)(\sigma_{//} - \sigma_{\perp}) \\ & + (\eta'_{//} - \eta'_{\perp}) = 0 \end{aligned} \tag{18}$$

It is important to point out that $\eta_{//}$ is a function of *r* seeing that creep strain normally varies in relation to the radius and therefore anisotropy also varies in relation to the radius.

The balance equation (9) can also be written as follows:

$$\sigma_{//} = \frac{r}{2}\frac{d\sigma_{\perp}}{dr} + \sigma_{\perp} \tag{19}$$

$$\sigma'_{//} = \frac{r}{2}\frac{d\sigma'_{\perp}}{dr} + \sigma'_{\perp} \tag{20}$$

or by differentiation in relation to *r*:

$$\frac{d\sigma_{//}}{dr} = \frac{3}{2}\frac{d\sigma_{\perp}}{dr} + \frac{r}{2}\frac{d^2\sigma_{\perp}}{dr^2} \tag{21}$$

$$\frac{d\sigma'_{//}}{dr} = \frac{3}{2}\frac{d\sigma'_{\perp}}{dr} + \frac{r}{2}\frac{d^2\sigma'_{\perp}}{dr^2} \tag{22}$$

By substituting (19) by (22) in (18) to exclude $\sigma_{//}$, the differential equation describing radial stress can be expressed as follows:

$$\frac{2r}{E}(1-\mu)\frac{d\sigma'_{\perp}}{dr} + \frac{r^2}{2E}(1-\mu)\frac{d^2\sigma'_{\perp}}{dr^2} + 2K(1-\nu)r\frac{d\sigma_{\perp}}{dr} + \frac{K(1-\nu)}{2}r^2\frac{d^2\sigma_{\perp}}{dr^2} - \eta' = 0 \tag{23}$$

with

$$\eta' = \eta'_{\perp} - \eta'_{//} - r\frac{d\eta'_{//}}{dr} \tag{24}$$

According to the following equation:

$$Y = 2r\frac{d\sigma_{\perp}}{dr} + \frac{r^2}{2}\frac{d^2\sigma_{\perp}}{dr^2}$$

the differential equation (23) can be written as follows:

$$\frac{(1-\mu)}{E}Y' + K(1-\nu)Y = \eta' \tag{25}$$

for which the solution is expressed as follows:

$$Y = e^{-Q}\int_0^{\gamma_0} e^{Q}\,\eta'\frac{E}{(1-\mu)}\,d\gamma \equiv f_K \tag{26}$$

with:

$$Q = \int_0^{\gamma_0} KE\frac{(1-\nu)}{(1-\mu)}\,d\gamma \tag{27}$$

It is important to remember that f_K is normally both a function of r and γ seeing that η' depends on r.

By changing the variable $r = \exp(z)$, it is demonstrated that the differential equation:

$$\frac{r^2}{2}\frac{d^2\sigma_{\perp}}{dr^2} + 2r\frac{d\sigma_{\perp}}{dr} = f_K$$

accepts the following solution:

$$\sigma_{\perp} = C_1 + \frac{C_2}{R^3} - \frac{2}{3}\frac{1}{R^3}\int_a^R r^2 f_K\,dr + \frac{2}{3}\int_a^R \frac{f_K}{r}\,dr \tag{28}$$

where R represents the radius of interest in the OPyC layer, and a represents its inner radius, while C_1 and C_2 represent two integration constants that can be determined based on the layer boundary conditions.

Based on the balance equation (9), the orthoradial stress can therefore be determined:

$$\sigma_{//} = C_1 - \frac{C_2}{2R^3} + \frac{1}{R^3}\int_a^R r^2 f_K\,dr + \frac{2}{3}\int_a^R \frac{f_K}{r}\,dr \tag{29}$$

3.2. SPECIFIC CASES WHERE f_K DOES NOT DEPEND ON THE RADIUS

Based on the assumption that $\eta_{//}$ and $\eta_{\perp}$ do not change in relation to the radius, then η' and consequently f_K (equation (26)) no longer depend on *r*, and equation (24) is written as:

$$\eta' = \eta'_{\perp} - \eta'_{//} \tag{30}$$

and equations (28) and (29) become:

$$\sigma_{\perp} = C_1 + \frac{C_2}{R^3} - \frac{2}{9R^3}\left[R^3 - a^3\right] f_K + \frac{2}{3}\ln\left(\frac{R}{a}\right) f_K \tag{31}$$

$$\sigma_{//} = C_1 - \frac{C_2}{2R^3} + \frac{2}{9R^3}\left[R^3 - a^3\right] f_K + \frac{2}{3}\ln\left(\frac{R}{a}\right) f_K \tag{32}$$

Based on the assumption that the OPyC layer is subject to pressure P_a on the inner wall and pressure P_b on the outer wall (radius *b*), the boundary conditions are:

$$\sigma_{\perp}(a) = -P_a \tag{33}$$

$$\sigma_{//}(b) = -P_b \tag{34}$$

where *b* represents the outer radius of the layer, which results in:

$$C_1 = -P_a - \left(\frac{b^3}{b^3 - a^3}\right)(P_b - P_b) + \frac{2}{9} f_K - \frac{2}{3} f_K \left(\frac{b^3}{b^3 - a^3}\right)\ln\left(\frac{b}{a}\right) \tag{35}$$

$$C_2 = \left(\frac{a^3 b^3}{b^3 - a^3}\right)(P_b - P_b) - \frac{2}{9} a^3 f_K - \frac{2}{3} f_K \left(\frac{a^3 b^3}{b^3 - a^3}\right)\ln\left(\frac{b}{a}\right) \tag{36}$$

This ultimately leads to the following stress equations:

$$\sigma_{\perp} = -\frac{a^3}{R^3}\frac{\left(b^3 - R^3\right)}{\left(b^3 - a^3\right)} P_a - \frac{b^3}{R^3}\frac{\left(R^3 - a^3\right)}{\left(b^3 - a^3\right)} P_b + \frac{2}{3}\left[\ln\left(\frac{R}{a}\right) - \frac{b^3}{R^3}\frac{\left(R^3 - a^3\right)}{\left(b^3 - a^3\right)}\ln\left(\frac{b}{a}\right)\right] f_K \tag{37}$$

$$\sigma_{//} = \frac{a^3}{2R^3}\frac{\left(2R^3 + b^3\right)}{\left(b^3 - a^3\right)} P_a - \frac{b^3}{2R^3}\frac{\left(2R^3 + a^3\right)}{\left(b^3 - a^3\right)} P_b + \frac{1}{3}\left[1 + 2\ln\left(\frac{R}{a}\right) - \frac{b^3}{R^3}\frac{\left(2R^3 + a^3\right)}{\left(b^3 - a^3\right)}\ln\left(\frac{b}{a}\right)\right] f_K \tag{38}$$

More specifically, by assuming $x = a/b$:

$$\sigma_{//}(a)=\frac{1}{2}\frac{\left(2x^3+1\right)}{\left(1-x^3\right)}P_a-\frac{3}{2}\frac{1}{\left(1-x^3\right)}P_b+\left[\frac{1}{3}+\frac{\ln(x)}{\left(1-x^3\right)}\right]f_K \tag{39}$$

$$\sigma_{//}(b)=\frac{3}{2}\frac{x^3}{\left(1-x^3\right)}P_a-\frac{1}{2}\frac{\left(2+x^3\right)}{\left(1-x^3\right)}P_b+\left[\frac{1}{3}+\frac{x^3}{\left(1-x^3\right)}\ln(x)\right]f_K \tag{40}$$

By referring to (16) and by identifying $\left[\frac{(1-\mu)}{E}f_K{}'+K(1-\nu)f_K\right]$ with η' (equation (25)), the following total tangential strain expressions according to a and b are obtained:

$$\begin{aligned}\varepsilon_{//}(a)&=\left[\frac{2}{3}-\frac{\ln(x)}{\left(1-x^3\right)}\right]\eta_{//}+\left[\frac{1}{3}+\frac{\ln(x)}{\left(1-x^3\right)}\right]\eta_{\perp}\\&+\int_0^{\gamma_0}\left\{K(1-\nu)\left[\frac{1}{2}\frac{\left(2x^3+1\right)}{\left(1-x^3\right)}P_a-\frac{3}{2}\frac{1}{\left(1-x^3\right)}P_b\right]+K\nu P_a\right\}d\gamma\\&+\int_0^{\gamma_0}\left\{\frac{(1-\mu)}{E}\left[\frac{1}{2}\frac{\left(2x^3+1\right)}{\left(1-x^3\right)}P'_a-\frac{3}{2}\frac{1}{\left(1-x^3\right)}P'_b\right]+\frac{\mu}{E}P'_a\right\}d\gamma\end{aligned} \tag{41}$$

$$\begin{aligned}\varepsilon_{//}(b)&=\left[\frac{2}{3}-\frac{x^3\ln(x)}{\left(1-x^3\right)}\right]\eta_{//}+\left[\frac{1}{3}+\frac{x^3\ln(x)}{\left(1-x^3\right)}\right]\eta_{\perp}\\&+\int_0^{\gamma_0}\left\{K(1-\nu)\left[\frac{3}{2}\frac{x^3}{\left(1-x^3\right)}P_a-\frac{1}{2}\frac{\left(2+x^3\right)}{\left(1-x^3\right)}P_b\right]+K\nu P_b\right\}d\gamma\\&+\int_0^{\gamma_0}\left\{\frac{(1-\mu)}{E}\left[\frac{3}{2}\frac{x^3}{\left(1-x^3\right)}P'_a-\frac{1}{2}\frac{\left(2+x^3\right)}{\left(1-x^3\right)}P'_b\right]+\frac{\mu}{E}P'_b\right\}d\gamma\end{aligned} \tag{42}$$

Based on the hypothesis that the pressures and x do not vary in time, these expressions therefore become:

$$\begin{aligned}\varepsilon_{//}(a)&=\left[\frac{2}{3}-\frac{\ln(x)}{\left(1-x^3\right)}\right]\eta_{//}+\left[\frac{1}{3}+\frac{\ln(x)}{\left(1-x^3\right)}\right]\eta_{\perp}\\&+\left(\frac{1}{2}\frac{\left(2x^3+1\right)}{\left(1-x^3\right)}P_a-\frac{3}{2}\frac{1}{\left(1-x^3\right)}P_b\right)\int_0^{\gamma_0}K(1-\nu)\,d\gamma+P_a\int_0^{\gamma_0}K\nu\,d\gamma\end{aligned} \tag{43}$$

$$\begin{aligned}\varepsilon_{//}(b)&=\left[\frac{2}{3}-\frac{x^3\ln(x)}{\left(1-x^3\right)}\right]\eta_{//}+\left[\frac{1}{3}+\frac{x^3\ln(x)}{\left(1-x^3\right)}\right]\eta_{\perp}\\&+\left(\frac{3}{2}\frac{x^3}{\left(1-x^3\right)}P_a-\frac{1}{2}\frac{\left(2+x^3\right)}{\left(1-x^3\right)}P_b\right)\int_0^{\gamma_0}K(1-\nu)\,d\gamma+P_b\int_0^{\gamma_0}K\nu\,d\gamma\end{aligned} \tag{44}$$

They are written as follows in the case where $P_a = P_b = P$:

$$\varepsilon_{//}(a)=\left[\frac{2}{3}-\frac{\ln(x)}{(1-x^3)}\right]\eta_{//}+\left[\frac{1}{3}+\frac{\ln(x)}{(1-x^3)}\right]\eta_{\perp}-P\int_0^{\gamma_0}K(1-2\nu)\,d\gamma \tag{45}$$

$$\varepsilon_{//}(b)=\left[\frac{2}{3}-\frac{x^3\ln(x)}{(1-x^3)}\right]\eta_{//}+\left[\frac{1}{3}+\frac{x^3\ln(x)}{(1-x^3)}\right]\eta_{\perp}-P\int_0^{\gamma_0}K(1-2\nu)\,d\gamma \tag{46}$$

and when ν = ½ (incompressibility of OPyC during creep) or P = 0, the expressions are simplified as follows (mixture laws):

$$\varepsilon_{//}(a)=\left[\frac{2}{3}-\frac{\ln(x)}{(1-x^3)}\right]\eta_{//}+\left[\frac{1}{3}+\frac{\ln(x)}{(1-x^3)}\right]\eta_{\perp} \tag{47}$$

$$\varepsilon_{//}(b)=\left[\frac{2}{3}-\frac{x^3\ln(x)}{(1-x^3)}\right]\eta_{//}+\left[\frac{1}{3}+\frac{x^3\ln(x)}{(1-x^3)}\right]\eta_{\perp} \tag{48}$$

It must be pointed out that **when *x* tends towards 1, $\varepsilon_{//}(a)$ and $\varepsilon_{//}(b)$ can be identified** vis-à-vis $\eta_{//}$, whereas when x tends towards 0 ($a \to 0$), the following is obtained:

$$\varepsilon_{//}(b)=\frac{2}{3}\eta_{//}+\frac{1}{3}\eta_{\perp} \tag{49}$$

In Reference *[10]*, J.L. KAAE *et al.* base their first-order reasoning on similar expressions without demonstration, namely:

$$\varepsilon_{//}(a)=\frac{1}{2}\left(\frac{1+x}{x}\right)\eta_{//}-\frac{1}{2}\left(\frac{1-x}{x}\right)\eta_{\perp}$$

$$\varepsilon_{//}(b)=\frac{1}{2}(1+x)\eta_{//}+\frac{1}{2}(1-x)\eta_{\perp}$$

which leads to numerical results that are practically identical to those obtained based on (47) and (48) when x is close to 1.

3.3. COMPARISON WITH THE ATLAS CODE

Version 2.1 of the ATLAS code was used to validate the analytical approach based on certain data sets resulting from Reference *[11]* in which E, K, ν and μ are systematically considered as a non-function of the fast fluence and $\eta'_{\perp}$, $\eta'_{//}$, provided in a polynomial form in relation to γ:

$$\eta'_{\perp} = a_0^{\perp} + a_1^{\perp}\gamma + a_2^{\perp}\gamma^2 + \ldots + a_n^{\perp}\gamma^n \tag{50}$$

$$\eta'_{//} = a_0^{//} + a_1^{//}\gamma + a_2^{//}\gamma^2 + \ldots + a_n^{//}\gamma^n \tag{51}$$

This results in the following expression (equation (30)):

$$\eta' = a_0 + a_1\gamma + a_2\gamma^2 + \ldots + a_n\gamma^n$$

where (52)

$$a_i = a_i^{\perp} - a_i^{//}$$

In this case, f_K is written as follows (equation (26)):

$$f_K = \frac{E}{1-\mu} e^{-\alpha\gamma} \int_0^{\gamma_0} e^{\alpha\gamma} \eta' \, d\gamma$$

or

$$f_K = \frac{E}{1-\mu} e^{-\alpha\gamma} \left[a_0 \int_0^{\gamma_0} e^{\alpha\gamma} d\gamma + a_1 \int_0^{\gamma_0} \gamma e^{\alpha\gamma} d\gamma + a_2 \int_0^{\gamma_0} \gamma^2 e^{\alpha\gamma} d\gamma + \ldots + a_n \int_0^{\gamma_0} \gamma^n e^{\alpha\gamma} d\gamma \right] \tag{53}$$

where

$$\alpha = K E \frac{1-\nu}{1-\mu}$$

The parameter α is expressed in terms of $[n/m^2]^{-1}$; it is more or less about $10^{-24}[n/m^2]^{-1}$.

The function f_K is therefore analytically solvable on the condition that the integral terms are also solvable through the recursive relationship:

$$\int \gamma^m e^{\alpha\gamma} d\gamma = \frac{\gamma^m e^{\alpha\gamma}}{\alpha} - \frac{m}{\alpha} \int \gamma^{m-1} e^{\alpha\gamma} d\gamma \tag{54}$$

Knowledge of x, P_a and P_b is used to calculate tangential and radial stresses (equations (37) and (38)), particularly internal and external tangential stresses $\sigma_{//}(a)$ and $\sigma_{//}(b)$ based on equations (39) and (40).

The following data were drawn from Reference *[11]* for comparison with the ATLAS V2.1[§] code:

E	μ	K	ν	$\eta'_{\perp}$ and $\eta'_{//}$
39600 MPa	0.33	2.715 10^{-4} [MPa $\cdot 10^{25}$ n/m^2 *(E>0.18 MeV)*]$^{-1}$	½	correlation (E)

[§] *Developed in the environment with CASTEM tools, ATLAS V2.1 does not make it possible any more than CASTEM to introduce creep coefficients differing by ½. Creep is therefore implicitly considered as isotropic and occurring at a constant volume (incompressibility).*

Analytical calculations were performed using MS Excel; more specifically, the f_K calculation was programmed as a recursive function in MS Excel/Visual Basic Applications. Concerning ATLAS and the buffer, options in terms of data input were chosen to simulate behaviour that is mechanically transparent to the latter.

COMPARISON FOCUSED ON TWO OPYC LAYER GEOMETRIES BASED ON **THE SAME THICKNESS OF 40 µM** AND TWO INNER RADIUSES (*A*) OF **420 µM** AND **1900 µM**, EQUIVALENT TO AN ***X*** OF **0.9130** AND **0.9794** RESPECTIVELY. THREE DIFFERENT CASES OF PRESSURE WERE TAKEN INTO ACCOUNT; ZERO PRESSURE, A PRESSURE OF 0.1 MPA (1 BAR), AND P_A = 0.072 MPA (0.72 BAR) AND P_B = 1 MPA (10 BARS). IN FIGURE 1 (A&B), FIGURE 2 (A&B) AND

figure 3 (A&B), inner and outer tangential stresses, as well as the analytically calculated entities $\Delta a/a$, $\Delta b/b$ and $\Delta e/e$ are compared to those calculated by ATLAS.

In any case, the changes corresponding to each of the different quantities versus the fast fluence make a satisfactory fit, which in principle confirms the analytical approach while validating (where appropriate) ATLAS mechanical modelling for BISO; this is the case for the ranges of x and pressures under investigation.

4. POTENTIAL OF EXPERIMENTAL EVALUATIONS ON BISO

Disregarding any problems of an experimental nature (conditions implemented to meet calculation hypotheses, uncertainties and measurement accuracy, etc.) in the beginning, the equations (43) and (44) have the potential of providing the following two options:

- Evaluating $\eta_{//}$ and $\eta_{\perp}$ based on knowledge of pressures and OPyC creep parameters with the specificity of being able to experimentally ignore the effect of pressure and therefore prior knowledge of creep parameters,

- Having access to creep parameters with known pressure, as well as $\eta_{//}$ and $\eta_{\perp}$ (or $\eta'_{//}$ and $\eta'_{\perp}$).

4.1. PARAMETERS $\eta_{//}$ & $\eta_{\perp}$

In principle and generally speaking, when it is possible to ignore the terms of equations (43) to (46) in which pressure is cited, the equations (47) and (48) have the potential of experimentally retrieving $\eta_{//}$ and $\eta_{\perp}$ if we know how to initially calculate x and measure changes in relation to both the outer radius

$\Delta b/b$ and the inner radius $\Delta a/a$ **or** the thickness (e = b-a) $\Delta e/e$ **or** the density of the OPyC layer through the following expressions:

$$\varepsilon_{//}(b) = \Delta b/b \quad (55)$$

$$\varepsilon_{//}(a) = \Delta a/a \quad (56)$$

$$\Delta e/e = \left(\frac{1}{1-x}\right)\Delta b/b - \left(\frac{x}{1-x}\right)\Delta a/a \qquad \text{(conservation of mass)}$$

or

$$\Delta e/e = \left[\frac{2}{3} + \frac{x(1+x)}{(1-x^3)}\ln(x)\right]\eta_{//} + \left[\frac{1}{3} - \frac{x(1+x)}{(1-x^3)}\ln(x)\right]\eta_{\perp} \quad (57)$$

by observing that $\Delta e/e \to \eta_{\perp}$ when $x \to 1$.

$$\frac{1}{1+\Delta d/d} = \left(\frac{1}{1-x^3}\right)(1+\Delta b/b)^3 - \left(\frac{x^3}{1-x^3}\right)(1+\Delta a/a)^3 \qquad \text{(conservation of mass)} \quad (58)$$

FIGURE 4 (A&B) AND

figure 5 (A&B) compare changes in relation to the fast fluence (respectively equivalent to x = 0.9130 and x = 0.9794, taking into account the same values as those used for previous parameters (see § 3.3), excepting ν equal to **0.3** or **0.4)** of the quantities $\Delta b/b$ and $\Delta e/e$ corresponding to several couples of pressure. It can be seen in these figures that **the contribution of pressure on these quantities is insignificant and can in fact be ignored**[**] **on the condition that P_a and P_b remain similar (about 0.1 MPa or 1 bar)**. Generally speaking, the effect of the P_a/P_b couple becomes more pronounced as x nears close to 1 (decrease in the layer stiffness), which proves to be more sensitive when ν decreases from 0.4 to 0.3 and clearly increases as the pressure rises.

However, even when contribution of pressure can be disregarded (the two first terms of equations (37) and (38)), it nevertheless remains that the self-generated contribution owing to anisotropic dimensional changes under irradiation and the spherical shell geometry of the OPyC layer become more accentuated (in terms of the maximum absolute tangential stress) as the parameter x moves away from 1 (see figure 6 (A&B)). Thus, an increase in the layer stiffness, with **the case of x = 1 being equivalent to a plane unrestrained system without biaxial stress gradients in the thickness**. The sensitivity of the coefficient K to change is demonstrated by the difference in stress levels reached between figure 6A and figure 6B (~ -45%). The sensitivity of the Young modulus is not as pronounced.

[**] *In principle, the most penalising P_a/P_b couple imaginable within the scope of this irradiation experiment is 0.072/0.1 MPa, which corresponds to a fuel particle manufactured under 1 bar at 1350 °C and irradiated at 900 °C.*

The direction change in the variation in $\eta_\perp$ (densification then orthoradial expansion) — sign of $\eta'_\perp$ with $\eta_{//}$ remaining stable (tangential densification) – can be mainly explained by the sign inversion of the internal and external stresses: the function f_K determines which fast fluence value will result in the stresses cancelling each other out.

Generally speaking, PyC strain rates due to irradiation ($\eta'_\perp$ and $\eta'_{//}$) are sensitive to PyC anisotropic changes (characterised by the Bacon anisotropy factor (BAF) or any other suitable quantity). This is a characteristic for which change is dependent on the state of stress, first in terms of the degree of triaxiality (or in this case, biaxiality) and then in terms of the intensity or sign. Consequently, changes in $\eta'_\perp$ and $\eta'_{//}$ (thus $\eta_\perp$ and $\eta_{//}$) in relation to time (i.e.: the fast fluence) are therefore related to the change in the state of stress. This actually challenges the hypothesis of the non-dependence of f_K with the radius seeing that the stresses vary locally. Nonetheless, in the case of PyC layers subject to slight or zero pressure, the intensity of self-generated biaxial stresses remain largely below (of a factor of about 10 or greater) the intensities reached with spherical or plane geometries in restrained conditions on the SiC layer (or any other) and graphite supports.

On the condition that microstructural representativeness is no longer a problem, the greater the mean diameter of the OPyC layer is, the more the effect of stress on $\eta'_\perp$ and $\eta'_{//}$ changes can be ignored. This means that it is more relevant to work on large particles rather than small ones. However, comparison of the behaviour of PyC layers corresponding to rather different particle sizes should provide – like many others – a great deal of useful information.

Note: In the presence of primary stress (i.e.: when pressures exist), the increase in the Young modulus (resulting from irradiation) theoretically contributes to elastic strain after irradiation and once stress relaxation has occurred. In terms of the recommended formalism, this strain is compared to permanent strain in OPyC. However, this contribution remains insignificant when pressures are low and similar.

4.2. PARAMETERS K AND ν

The formalism of the equations (43) and (44) allows for different possibilities when experimentally evaluating these more or less problematic parameters depending on whether the $\eta_{//}$ & $\eta_\perp$ changes in relation to the fluence have already been determined or not. Using the second possibility requires taking into account the fact that $\eta_{//}$ & $\eta_\perp$ changes versus the fluence do not significantly vary in relation to the different pressure loads in question.

4.2.1. Previously determined $\eta_{//}$ & $\eta_{\perp}$ changes

Let $I(\gamma_0) = \int_0^{\gamma_0} K(1-\nu)\,d\gamma$ and $J(\gamma_0) = \int_0^{\gamma_0} K\nu\,d\gamma$.

In the case of BISO-coated fuel particles having integrated the same fluence γ_0 and "operating under" a constant and known pressure couple (P_a being the internal pressure inherent to both fabrication and the operating temperature, while P_b is the external pressure), the experimental determination of both $\Delta b/b$ and $\Delta a/a$, coupled with the knowledge of x and variations in $\eta_{//}$ et $\eta_{\perp}$ with the fluence, generally makes it possible to deduce the integral terms (γ_0) and $J(\gamma_0)$ of equations (43) and (44). It may even be possible to directly infer K and ν if they are not a function of the fluence. Generally speaking, the iteration of this procedure with γ_0 as the parameter therefore makes it possible to obtain the variations in I and J in relation to γ, before differentiation with $K(\gamma)$ and $\nu(\gamma)$.

If the hypothesis of non-variation of $\eta_{//}$ and $\eta_{\perp}$ in relation to the state of stress is considered acceptable, the method only requires knowledge of "unrestrained variations" in these entities.

Otherwise, following the example of what is used for plane geometry and without going into details, the procedure (to be repeated as many times as necessary) may consist in irradiating a group of fuel particles with pressures required to determine K and ν for a given time, before characterising this group, and then continuing irradiation in unrestrained conditions. In the end, we would obtain changes in relation to $\eta'_{//}(\gamma)$ and $\eta'_{\perp}(\gamma)$ taking into account – all things being equal – the microstructural variation in PyC.

4.2.2. Case of $\eta_{//}$ & $\eta_{\perp}$ being independent from pressure loads

Based on the hypothesis of two groups of BISO-coated fuel particles having integrated the same fluence γ_0 that share the same internal pressure P_a (pressure inherent to fabrication and the operating temperature) but that are subject to two different and constant external pressures, P_b^0 and P_b^1, the following equations can be written:

$$\varepsilon^1_{//}(b) - \varepsilon^0_{//}(b) = \Delta(\Delta b/b) = \left[A(x)\,I(\gamma_0) + J(\gamma_0)\right]\left(P^1_b - P^0_b\right)$$

$$\varepsilon^1_{//}(a) - \varepsilon^0_{//}(a) = \Delta(\Delta a/a) = B(x)\,I(\gamma_0)\left(P^1_b - P^0_b\right)$$

where

$$A(x) = -\frac{1}{2}\frac{\left(2+x^3\right)}{\left(1-x^3\right)},\quad B(x) = -\frac{3}{2}\frac{1}{\left(1-x^3\right)},\quad I(\gamma_0) = \int_0^{\gamma_0} K(1-\nu)\,d\gamma \quad \text{et} \quad J(\gamma_0) = \int_0^{\gamma_0} K\nu\,d\gamma$$

Of course, similar expressions can be obtained by inverting the role of internal and external pressures.

By knowing the values of x and external pressures in addition to strain differences, it is theoretically possible to obtain the integral terms $I(\gamma_0)$ and $J(\gamma_0)$ based on the two previous equations. It is even possible to obtain K and ν if they are not a function of the fluence. This also makes it possible to infer $\eta_{//}$ and $\eta_{\perp}$ values taking into account the state of stress in question. The iteration of this procedure using γ_0 as the parameter also makes it possible to calculate variations in I and J in relation to γ, before differentiation with $K(\gamma)$ and $\nu(\gamma)$.

figure 7 (A&B) compares changes in relation to the fast fluence, respectively for $x = 0.9130$ and $x = 0.9722$, of the quantities $\Delta(\Delta b/b)$ and $\Delta(\Delta a/a)$ calculated analytically based on the above-mentioned equations corresponding to three P_a / P_b^1 couples (P_a = constant = 0.085 MPa) relative to the couple $P_a / P_b^0 = 0{,}085/0{,}1$ MPa. Once again, these equations take into account the same values of the previously-mentioned parameters (see § 3.3), excluding ν which is equal to 0.4. More specifically, substantial pressure differences and large diameters are required to evaluate K and ν.

4.2.3. Relevance of a pressure approach and related experimental problem

Using pressure as the main force driving creep normally makes it possible to control (and stabilise) and quantify the state of stress, according to the distribution of the internal and external pressures undergoing compression or tension. A correlation of the "state of integrated stress - degree of resulting anisotropy" does seem possible based on the assumption that the phenomena are decoupled. This in turn would make it possible to use correlations based on the "degree of anisotropy - $\eta'_{//}(\gamma)$, $\eta'_{\perp}(\gamma)$". The most appropriate stress "evaluator" (tangential stress, etc.) remains to be determined for the characterisation of the stress system relative to anisotropy. The effect of the size of the fuel particle in terms of the microstructure may also be studied through changes in $\eta_{//}$ and $\eta_{\perp}$ (x parameter).

Insofar as PyC is not supposed to be leaktight, one of the experimental problems to be solved involves pressurising and maintaining the internal and external pressures at a constant and predetermined level. This means either rendering the surface leaktight or transferring pressure via an impermeable membrane that is mechanically transparent (see Reference *[12]*).

In principle, it seems much easier to generate and control external pressures than internal pressures. Furthermore, the option involving control via the internal pressure may require (pressure is not determined by simply increasing the temperature) drilling holes in the particles to relax elastic stresses after irradiation and before possibly resuming "unrestrained" irradiation on the same particles.

However, in the case where conditions are controlled via the external pressure, the problem of potential buffer shrinkage is accentuated because the decrease in the OPyC inner diameter is amplified.

5. IRRADIATION EXPERIMENT OPTIONS

Even though the fuel particle approaches involving pressure seem to have a greater potential in providing accessible data (at least in terms of this document), the related experimental problem needs more extensive research especially in terms of uncertainties before an irradiation experiment as described in § 4.2 can be reasonably considered in the short term.

However, the experimental approach such as that described in § 4.1 seems technically plausible, not to mention relatively and rapidly feasible. Though this approach reaches its limit when it comes to determining unrestrained or practically unrestrained $\eta_{//}$ and $\eta_{\perp}$ (moderate self-generated biaxial stresses), this does not make it any less relevant (particularly when compared with “earlier” PyC fabrications), insofar as the vast majority of formalisms available in literature neither mention nor integrate changes that are a function of the anisotropic variation. This is all the more so true because like other fuel particle thermohydraulic codes, the ATLAS code implicitly establishes the hypothesis according to which the entities $\eta_{//}$ and $\eta_{\perp}$ do not vary in relation to *r*, i.e.: in relation to the state of stress, or in other words, in relation to the anisotropic changes – through lack of a suitable correlation, which has been questioned several times in this document.

The experimental study of practically unrestrained dimensional changes in the spherical PyC layers was therefore chosen as the **main theme** for this part of the PYCASSO irradiation experiment. The various different theoretical elements and the experimental problem that have been raised or briefly mentioned led to the proposal of an irradiation experiment to be performed on two different sizes of particles based on inert kernels with respective diameters of 500 µm and 2000 µm. It was decided to study one OPyC layer thickness only to avoid multiplying parameters.

In addition, the particles including a SiC layer with identical kernel diameters will be irradiated simultaneously, with the following objectives in mind:

- Obtaining information on the ductility of PyC under irradiation and with load conditions that are representative of normal operation (heavy biaxial load), knowing that ductility is not an inherent characteristic,
- Quantifying SiC swelling,
- Assessing the difference between unrestrained swelling (no OPyC layer) and restrained swelling (compression) of SiC (OPyC layer) using a representative spherical geometry,
- Comparing geometrical changes in this type of particle with ATLAS numerical calculations (integrating experimental data resulting from irradiation).

Compliance with the hypothesis based on the non- “Buffer-OPyC Mechanical-Interaction” (BOPMI)[††] depends on the buffer’s capacity to densify under irradiation and/or disintegrate, crumble or compact owing to external stress without any significant resistance. For this reason, kernel-buffer type fuel particles will also be irradiated with the aim of checking the validity of this hypothesis. On an independent basis, examination of these particles will provide information on densification-compaction kinetics and microstructural buffer changes. Complying with this hypothesis also requires taking into account kernel swelling, which is an integral part of its nature.

The buffer thickness in relation to kernel behaviour therefore determines its shrinkage potential and consequently the overall particle diameter, but especially the maximum irradiation time that is compatible with the above-mentioned hypothesis (non-BOPMI).

5.1. BUFFER SHRINKAGE POTENTIAL

5.1.1. Inert kernel material

The following criteria need to be taken into account when choosing a material for the kernel:

– Density: the objective is to avoid departing from parameters generally required when making fuel particles (specified density of 10.5 for the UO_2 kernel)

– Post-irradiation activity: possibility of post-irradiation handling in a glove box when the activity level has dropped (which is problematic in terms of material-related impurities)

– Swelling under irradiation,

– Temperature stability particularly in terms of possible phase changes,

– Non-generation of fission gases such as helium,

– Compatibility with reactor management,

– Commercial availability.

[††] *Interaction **M**écanique **B**uffer **OP**yC in French (translator’s note)*

The table below provides the densities of possible materials:

SiC	Al_2O_3-α polycrystalline alumina	Al_2O_3-α corundum	$ZrO_2(HfO_2)/Y_2O_3$ Y-TZP (YTZ)	HfO_2 hafnium oxide
~3.2	3.9 – 4.1	3.99	5.95 – 6.0	9.7 – 9.9

It is worth pointing out that corundum (sapphire) has been the most frequently-used material by HTR experimenters and therefore has the most feedback, which makes it the most industrially-available material, with a very low total content of impurities (low activation), i.e.: 99.99% of aluminium sesquioxide according to the CIMAP company.

5.1.2. Irradiation time before BOPMI

Based on the assumption that total buffer compaction results in a relatively **homogeneous and isotropic** variation in density $\Delta d/d$ on the one hand, and volume swelling $\Delta V/V$ (written G) of the inert kernel with an initial diameter $Ø$ on the other hand, the relative variation associated with the outer buffer radius $\Delta a/a$ (a also being the initial inner radius of the OPyC layer) is written as follows:

$$\Delta a/a = \left[(1-k)+(k+G)\left(\frac{Ø}{2a}\right)^3\right]^{1/3} - 1 \qquad (59)$$

with $1-k = \dfrac{1}{1+\Delta d/d}$

or

$$1-k = \frac{1-p}{1-p^*}$$

where p and p^* represent the porosities before and after buffer compaction respectively.

In the case where compaction can be identified by volume densification inherent under irradiation $\Delta V/V$ (written D), the following expression applies:

$$\Delta a/a = \left[(1+D)+(G-D)\left(\frac{Ø}{2a}\right)^3\right]^{1/3} - 1 \qquad (60)$$

The maximum compaction corresponds to the theoretical case where the buffer reaches its theoretical density ($p^* = 0$, or $D = -p$), which means equation (59) can be expressed as follows:

$$\Delta a/a = \left[(1-p)+(p+G)\left(\frac{Ø}{2a}\right)^3\right]^{1/3} - 1 \qquad (61)$$

Before setting a plausible maximum irradiation time prior to BOPMI or at least before geometrical overlapping occurs between the OPyC layer shrinkage and the buffer, we compared changes versus the fast fluence for 1) relative variations in the buffer outer radius estimated using equation (60) and 2) variations in the inner radius of the OPyC layer (material data identical to those given in § 3.3), in both cases written as $\Delta a/a$:

– By exclusively taking into account buffer densification resulting from irradiation (penalising approach),

– With and without kernel swelling: based on the normally maximum volume swelling of the previously listed buffer materials, i.e.: Al_2O_3-α (extrapolated beyond the temperature qualification range: 387°C – 827°C) [13],

– Based on the three expressions for isotropic densification laws provided in the technical note [14 : FZJ, BNFL and CEGA,

– Based on two kernel-buffer couples that are theoretically experimentally feasible, *Ø*/*a*: 500/170 µm and 2000/400 µm.

In terms of the **fast fluence** ($10^{-25} \cdot \gamma [n/m^2]$ – E > 0.18 MeV), the maximum irradiation times are as follows:

	G = 0	*G* (827 °C)	*G* (900 °C)	*G* (1000 °C)	*G* (1100 °C)	*G* (1200 °C)	*G* (1300 °C)
500/170 µm	3.0	2.8	2.8	2.7	2.6	2.4	2.3
2000/400 µm	2.4	2.2	2.1	2.0	1.8	BOPMI limit from the start (CEGA)	BOPMI limit from the start (CEGA)

figure 8 (A&B) and figure 9 (A&B) illustrate the changes in $\Delta a/a = f(\gamma)$, which respectively correspond to 500/170 µm and 2000/400 µm for *G* = 0 (A) and *G*(1100 °C) (B). Beyond the CEGA interaction, the FEJ law systematically proves to be design-based in terms of BOPMI.

Based on the assumption that the maximum integral neutron flux is greater than 0.18 MeV in position G3[‡‡] of the HFR with a dummy aluminium element in this position (see figure 10), which is equivalent to 1.882 $\cdot 10^{18}$ n/m^2/s, the threshold limits in terms of effective full power days (EFPD) are as follows:

	G = 0	*G* (827 °C)	*G* (900 °C)	*G* (1000 °C)	*G* (1100 °C)	*G* (1200 °C)	*G* (1300 °C)
500/170 µm	185	172	172	166	160	148	141
2000/400 µm	148	135	129	123	111	BOPMI limit from the start (CEGA)	BOPMI limit from the start (CEGA)

In a conservative manner, the objective is to obtain a maximum buffer porosity, that is to say, at least the lower bound of specifications in terms of density, i.e.: *d* = 0.9, or *p* = 59.46% based on a theoretical PyC density of 2.22. This is necessary to obtain a buffer manufacturing range that is considered representative.

5.2. PARTICLE TYPES

This irradiation experiment does not intend to investigate the effect of the microstructure on the behaviour of PyC and SiC. This experiment aims to correspond with UO_2 fuel particle specifications, which are: respective thicknesses of 40 µm and 30µm, respective densities of 1.90 and ≥ 3.18, and a OPyC BAF of ≤ 1.04.

Four types of particles in two different sizes were finally recommended for irradiation: 2 dedicated to studying PyC behaviour and 2 with a SiC layer.

	kernel/buffer/PyC	kernel /buffer	kernel /buffer/SiC	kernel /buffer/SiC/PyC
Ø/ thickness *[µm]* scale: x 10 and real size in *A4* format	500/170 	500/170/40 	500/135/35 	500/135/35/40 
	2000/400 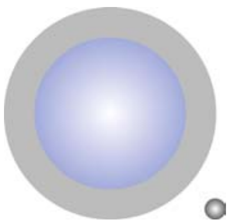	2000/400/40 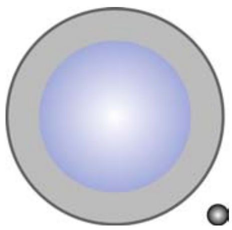	2000/365/35 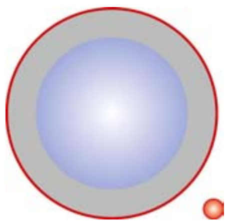	2000/365/35/40 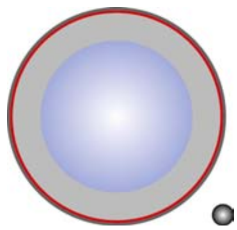

[‡‡] *Energy fluences > 0.10 MeV are obtained in this position by multiplying energy fluences > 0.18 MeV by 1.0915.*

6. ASSESSMENT AND EVOLUTION OF UNCERTAINTIES

Considering errors as independent and theoretically comparing them to small algebraic increases, a literal assessment of uncertainties was carried out based on the experimental evaluation of $\eta_{//}$ and $\eta_{\perp}$ on the basis of explicit dependence relationships:

$$\eta_{//} = \left[1 + \frac{1}{3\ln(x)} + \frac{x^3}{(1-x^3)}\right]\Delta b/b - \left[\frac{1}{3\ln(x)} + \frac{x^3}{(1-x^3)}\right]\Delta a/a \tag{62}$$

$$\eta_{\perp} = \left[1 - \frac{2}{3\ln(x)} + \frac{x^3}{(1-x^3)}\right]\Delta b/b + \left[\frac{2}{3\ln(x)} - \frac{x^3}{(1-x^3)}\right]\Delta a/a \tag{63}$$

resulting from the equations (47) and (48), which can be simplified as follows:

$$\eta_{//} = A_{//}\ \Delta b/b + (1 - A_{//})\Delta a/a \tag{64}$$

$$\eta_{\perp} = A_{\perp}\ \Delta b/b + (1 - A_{\perp})\Delta a/a \tag{65}$$

with $A_{//}$ and $A_{\perp}$ being positive.

By expressing the absolute uncertainties on $\eta_{//}$ and $\eta_{\perp}$ in terms of $\delta\eta_{//}$ and $\delta\eta_{\perp}$, and based on the assumption that $A_{//}$ and $A_{\perp}$ are constant (x constant), the following is established:

$$\delta\eta_{//} = A_{//}\ \delta(\Delta b/b) + |1 - A_{//}|\ \delta(\Delta a/a) \tag{66}$$

$$\delta\eta_{\perp} = A_{\perp}\ \delta(\Delta b/b) + |1 - A_{\perp}|\ \delta(\Delta a/a) \tag{67}$$

6.1. RADIUS AND THICKNESS MEASUREMENTS

Let δb be the absolute uncertainty **common to dimensional measurements of radiuses** or thicknesses, then the absolute uncertainties on $\eta_{//}$ and $\eta_{\perp}$ are expressed according to the **formalism of this document**:

$$\delta\eta_{//} = \delta b\left[\frac{A_{//}}{b}(2 + \Delta b/b) + \frac{|1 - A_{//}|}{a}(2 + \Delta a/a)\right] \tag{68}$$

$$\delta\eta_{\perp} = \delta b\left[\frac{A_{\perp}}{b}(2 + \Delta b/b) + \frac{|1 - A_{\perp}|}{a}(2 + \Delta a/a)\right] \tag{69}$$

6.2. RADIUS AND DENSIMETRIC MEASUREMENTS OF THE OPYC LAYER

The equation (58) can be expressed as follows:

$$\frac{1}{1+\Delta d/d} = A_d\left(1+\Delta b/b\right)^3 + \left(1-A_d\right)\left(1+\Delta a/a\right)^3 \tag{70}$$

In the case where determining $\Delta a/a$ is based on measuring the relative variation in density $\Delta d/d$ (as applied to plane geometry), the following is reached:

$$\delta\eta_{//} = \frac{\delta b}{b}\left(2+\Delta b/b\right)\left[A_{//} + \left|\frac{A_d}{1-A_d}\right|\left(\frac{2+\Delta b/b}{2+\Delta a/a}\right)^2\right] + \frac{1}{3}\left|\frac{1-A_{//}}{1-A_d}\right|\frac{\delta d}{d}\frac{\left(2+\Delta d/d\right)}{\left[\left(1+\Delta d/d\right)\left(1+\Delta a/a\right)\right]^2} \tag{71}$$

$$\delta\eta_{\perp} = \frac{\delta b}{b}\left(2+\Delta b/b\right)\left[A_{\perp} + \left|\frac{A_d}{1-A_d}\right|\left(\frac{2+\Delta b/b}{2+\Delta a/a}\right)^2\right] + \frac{1}{3}\left|\frac{1-A_{\perp}}{1-A_d}\right|\frac{\delta d}{d}\frac{\left(2+\Delta d/d\right)}{\left[\left(1+\Delta d/d\right)\left(1+\Delta a/a\right)\right]^2} \tag{72}$$

where δd represents absolute uncertainty **common to density measurements**.

In consideration of the normal values of δd, the second term of these expressions proves to be practically negligible in comparison to the first.

6.3. NUMERICAL APPLICATIONS

This exercise involves comparing uncertainty estimates resulting from the equations (68) and (69) with those resulting from (71) and (72). This is done by considering the analytical estimates based on (47) and (48) as experimental values of $\Delta a/a$ and $\Delta b/b$. OPyC data from § 3.3 was used: (with d = 1.9), for x = 0.9130 (500 µm kernel) & x = 0.9722 (2000 µm kernel) and for d = 1.9, δd = 0.0001 & δb = 0.5 µm (theoretically common values).

figure 11 compares variations in the relative uncertainty $\delta\eta/|\eta|$ ($_{//}$ and $_{\perp}$) — calculated on the basis of the correlation (E) — in relation to the fast fluence for the eight possible cases. This figure clearly shows (even if the hypothesis based on comparing errors to small increases is not really systematically justified):

- the advantage of large diameters (2000 µm kernel) when it comes to experimentally determining $\eta_{//}$,
- the need to use densimetry when referring the densimetry of $\eta_{\perp}$.

Between 0.3 ·10^{25} n/m^2 and 2.5 ·10^{25} n/m^2, uncertainty on $\eta_{//}$ is still acceptable, whereas uncertainty on $\eta_{\perp}$ remains borderline even in the best of conditions. Insofar as uncertainties are directly proportional to δb, minimising the latter parameter still remains relevant.

It is nevertheless important to point out that the effect of $\eta_{\perp}$ uncertainty on stress evaluation is much less than that on $\eta_{//}$, considering that it is the latter that determines the level of biaxial stress in a standard TRISO configuration. The analytical expression of $\sigma_{//}$ (hypotheses identical to those in § 3.2 and 3.3) corresponding to the case of a restrained PyC layer on a plane support (infinite-radius sphere) is proof of this, as shown below:

$$\sigma_{//} = -\frac{E}{1-\mu} e^{-\alpha\gamma} \int_0^{\gamma_0} e^{\alpha\gamma} \eta'_{//} \, d\gamma$$

where the entity $\eta'_{//}$ only is used.

6.4. EFFECT OF VARIATION IN *X*

The orders of magnitude of this effect are estimated based on a numerical example.

Relative uncertainty in determining *x* is given by: $\frac{\delta x}{x} = \frac{\delta a}{a} + \frac{\delta b}{b}$. For δb = δa = 0.5 µm, its value is equal to 0.228 % and 0.070 % for small and large particles respectively.

For the interval $0 - 2.5{\cdot}10^{-25}{\cdot}\gamma\,[n/m^2]$ (E > 0.18 MeV), dimensional changes that are analytically estimated based on data in § 6.3 result in a maximum relative variation in the parameter *x* equivalent to 0.297% and 0.092% for small and large particles respectively. In a conservative manner, the accumulation of these two sources of approximation leads to a multiplicative factor of x equivalent to 1.00525/0.99475 and 1.00162/0.99838 respectively, which results in the following maximum relative uncertainties (all else being equal):

$\frac{\delta \eta_\perp}{|\eta_\perp|} = 4{,}70\ \%$ and $\frac{\delta \eta_{//}}{|\eta_{//}|}$ negligible, all sizes included.

6.5. PROPOSAL OF A DIMENSIONAL MEASUREMENT METHOD

Within the scope of a statistical approach of behaviour, one method consists in measuring the mean diameter of a sufficient number of fuel particles in a global manner. A way of doing this consists in lining up the particles in a V-shaped tray for which the longitudinal axis is slightly inclined so that the adjacent particles are in contact and the length of this stack can be measured several times. The particles are in a different order and position each time. If the fuel particle diameters are dissimilar, the mean diameter measured will also be less than the real diameter.

Based on certain simplified yet penalising hypotheses for which the population is exclusively composed of *n* particles of two extreme diameters (*R* – upper bound and *r* – lower bound) and for which two geometries regularly alternate within the stack, the systematic relative error *F* of the method used to evaluate the mean diameter can therefore be expressed as such *[15]*:

$$F = \frac{\O - \bar{\O}}{\bar{\O}} = -\left(1 - \frac{1}{n}\right)\left[1 - \sqrt{1 - \frac{(R-r)^2}{(R+r)^2}}\right] \tag{73}$$

where Ø is the smallest commensurable diameter and $\bar{\O} = R + r$.

Error is less significant in all other geometry scenarios than the one described above.

In order to establish the orders of magnitude and in the case an absolute uncertainty of 1 µm on the stack length is accessible, applying this method to geometries and n values specified in § 8 results in the following absolute uncertainties on the following radiuses (to be compared with δb = 0.5 µm):

$\O_p$ - n	R - r = 20 µm	R - r = 30 µm	R - r = 40 µm	R - r = 50 µm	R - r = 60 µm	R - r = 70 µm
840 µm - 111	0.12 µm	0.27 µm	0.48 µm	> 0.5 µm	> 0.5 µm	> 0.5 µm
920 µm - 111	0.11 µm	0.25 µm	0.44 µm	> 0.5 µm	> 0.5 µm	> 0.5 µm
2800 µm - 30	0.05 µm	0.09 µm	0.15 µm	0.23 µm	0.33 µm	0.44 µm
2880 µm - 30	0.05 µm	0.09 µm	0.15 µm	0.23 µm	0.32 µm	0.43 µm

This shows it is possible to reduce uncertainty by a significant factor using an experimental approach based on the selection of fuel particles coupled with “global” measurements.

7. STATISTICAL ASPECTS

Seeing that a global approach has been chosen, i.e.: the particles are not experimentally discernible, a sufficient number n of the same type of particles must be treated under identical irradiation conditions (fluence and temperature) to be characteristics of the behaviour of all particles. For statistical treatment, a number $n \geq 50$ corresponds to the minimum size required so that a sample can be considered representative of a population. To establish the orders of magnitude, a reactor load (reaction oven) of 500 g corresponds to 1,914,646 kernels Ø = 500 µm and 29,916 kernels Ø = 2000 µm composed of corundum (kernel density of 3.99).

Minimising uncertainties – particularly those related to determining $\eta_\perp$ – requires limiting the choice of fuel particle external diameters, which justifies raising the question as to the representativeness of this specific selection. However, for any given order of magnitude, it seems reasonable to believe that the spectrum of particle sizes only reflects that of inert kernels, which does not have a significant effect on the microstructure.

Considering it is necessary to obtain homogeneous behaviour and thus homogeneous manufacturing, the recommended approach consists in choosing kernels so as to obtain the most accurate distribution histogram in diameters and carry out selection during all sampling phases of the manufacturing process according to the same criteria. The number of fuel particles per load permits the excessive sampling of particles at each phase while avoiding significant modification of the load mass. This is normally sufficient in order to establish the number of homogeneous particles to be distributed into two batches: one for irradiation and the other for statistical characterisation prior to irradiation. All disregarded particles may possibly be reintroduced into the reactor.

8. DRUM COMPOSITION

The main constraints related to the drums are their adequacy vis-à-vis the hypotheses governing the possibility of experimentally determining $\eta_{//}$ and $\eta_{\perp}$ and the statistical representativeness (fuel particle samples) in view of the maximum overall dimensions imposed by the HFR experimental device at Petten, such as:

- The space available per cylindrical drum (stress on the minimum metallic mass required for heating), i.e.: per flux zone and/or homogeneous temperature;
- Available diameter, ***D***, of **21 mm** (22.5 mm effective diameter) and height, ***H***, overall size of **50 mm**, to be reconciled with the two particle sizes (see arguments reported in § 4.1).

Hexagonal cross section cavities were chosen (fuel particle box), with a distance across flats of $D\cdot\sqrt{3}/2$, coherent with a **planar arrangement (single layer) of compact, hexagonal-type particles**, which is in principle more appropriate for a homogeneous distribution of temperatures (and fluences) while being capable of preventing mechanical interactions (inter-particle restraint, minimisation of contacts and friction); this is also based on the principle that the plane, side walls of cavities will encourage a well-ordered structure of the single layers composed of fuel particles.

Based on this geometry and considering fuel particles with a diameter $\varnothing_p$, the maximum acceptable number of rings of particles p is given by the **integer value** of the following expression:

$$\frac{D}{2\varnothing_p}-\frac{1}{\sqrt{3}}$$

the maximum number n of particles therefore provided by (p = 0 corresponding to one particle only):

$$n=1+3p(p+1)$$

The application of these relationships for the four particle types results in the following counts and maximum acceptable diameters:

Type	Ø/ thicknesses *[µm]*	$Ø_p$ *[µm]*	*p*	*n*	maximum $Ø_p$ *[µm]*	Tray
kernel/buffer	500/170	840	12	397	906.94	P_{P2}
kernel /buffer/OPyC	500/170/40	920	11	331	992.69	P_{P1}
kernel /buffer	2000/400	2800	3	37	2935.13	P_{G2}
kernel /buffer/OPyC	2000/400/40	2880	3	37	2935.13	P_{G1}
kernel /buffer/SiC	500/135/35	840	12	397	906.94	P_{P2}
kernel /buffer/SiC/OPyC	500/135/35/40	920	11	331	992.69	P_{P1}
kernel /buffer/SiC	2000/365/35	2800	3	37	2935.13	P_{G2}
kernel /buffer/SiC/OPyC	2000/365/35/40	2880	3	37	2935.13	P_{G1}

Finally and taking into account space required for temperature sensors, the drum volume is decoupled into 14 cylindrical stages, with 2 solid stages at both ends (plugs, B) and 12 stages (trays) of particles distributed in the following manner:

– 8 trays (4 P_{G1} and 4 P_{G2}, equivalent to 2 trays per particle type) each housing a hexagonal cavity with a distance between flats of $21{\cdot}\sqrt{3}/2$ mm truncated on two adjacent sides, holding 29 to 30 large beads (depending on whether there is a central fuel particle or not) of the type kernel/buffer, kernel /buffer/OPyC, kernel /buffer/SiC or kernel /buffer/SiC/OPyC,

– 2 trays (P_{P1}) including 3 hexagonal cavities with a distance between flats of $7{\cdot}\sqrt{3}/2$ mm each containing 37 small beads, equivalent to 111 particles of the type kernel/buffer/OPyC or kernel /buffer/SiC/OPyC per tray,

– 2 trays (P_{P2}) including 3 hexagonal cavities with a distance between flats of $6{,}5{\cdot}\sqrt{3}/2$ mm each containing 37 small beads equivalent to 111 of the type kernel/buffer or kernel/buffer/SiC per tray.

The trays all have a 1 mm thick solid base; the trays P_G and P_P have a total height of 4.10 and 2.10 mm respectively; the plugs are 4.40 mm high.

The partitioned trays P_{P1} and P_{P2} should simplify the handling of small particles (positioning inside the cavities). The cavity dimensions are such that the particle diameter may systematically exceed a maximum of 55 µm (large) or 60 µm (small).

These parameters are shown in the diagrams (scale of 1 based on an A4 format) below:

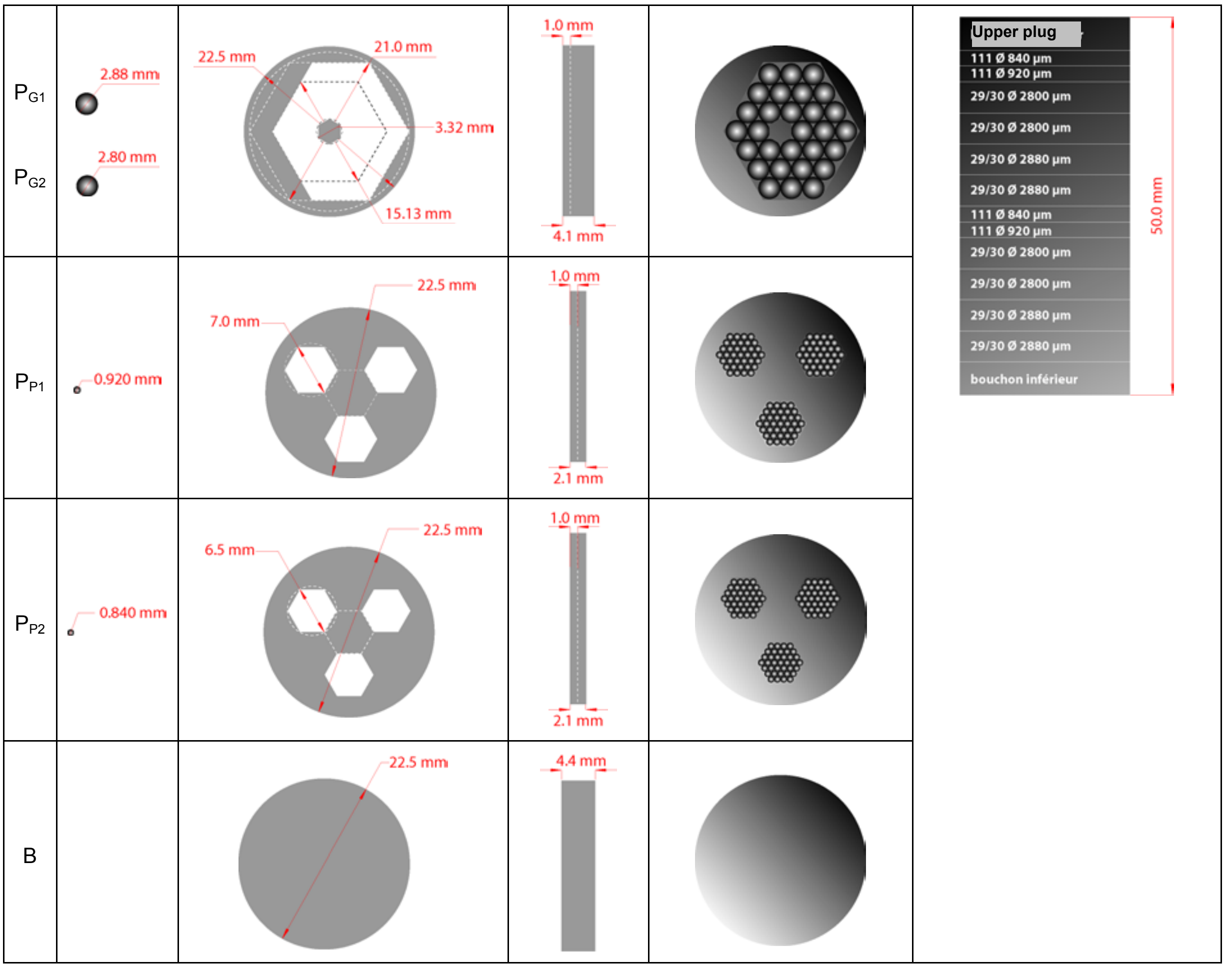

Owing to the deposited power γ required by the temperature levels (heating), the material composing the trays is the molybdenum-based alloy TZM (Mo-0.5Ti-0.08Zr-[0.1-0.4]C in at.%); a coating or strip (several µm thick) composed of a material yet to be defined shall be used to prevent any chemical reaction with the outer particle coating (buffer, OPyC or SiC). Rhenium (possibly coupled with graphite) has been suggested owing to its compatibility with silicon carbide up to 1600°C *[16]* and graphite up to at least 1100°C *[17]*. The conditions of its efficiency as a barrier material nevertheless remain to be checked and specified, i.e.: effects of the microstructure and the thickness *[18]*.

In terms of preserving the mechanical integrity of the fuel particles, the chosen dimensions are largely conservative insomuch as the particles will decrease in diameter and the thermal expansion of TZM is greater than particle thermal expansion.

9. CHARACTERISATION AND POST-IRRADIATION EXAMINATIONS

Performing this irradiation experiment requires at the least:

- Microstructural characterisation of the different types of layers and measurement of the OPyC anisotropy using BAF or any other anisotropy factor (comparison between the two mean deposit diameters);

- Determining the mean diameter of each fuel particle type before and after irradiation;

- Determining the mean density of the different layers of each particle type before and after irradiation.

If the method used to determine the mean diameters is a global one, it will nonetheless be based on individual measurements – during sorting for example – so as to quantify the scope of diametral dispersion in the batches.

As density measurements are destructive, they will be performed:

- On the batch of fuel particles intended for characterisation before irradiation (see § 7) and on a greater number of particles than the number of irradiated particles of the same type (for statistical needs); as density measurements are individual, it will be necessary to evaluate dispersion (standard deviation),

- On the entire batch (when possible) after irradiation.

Pre- and post-irradiation statistical measurements of the mean outer diameters of the kernel/buffer beads (a) and the kernel/buffer/OPyC beads (*b*) are used to determine the value of *x* and its variation under irradiation. Pre- and post-irradiation statistical measurements of the mean outer diameter of kernel/buffer/OPyC beads, coupled with statistical measurements of the mean density of OPyC, are used to determine $\eta_{//}$ and $\eta_{\perp}$.

However, determining Young's modulus and Poisson's ratio would at least make it possible to update the experimental results using the ATLAS code insofar as the other part of the PYCASSO experiment evaluates creep parameters.

10. IRRADIATION PARAMETERS

In order to obtain experimental results corresponding to several different fast fluences at a given temperature, the 400 mm long PYCASSO rig will house four 90 mm high containers. At least 3 drums will be irradiated as described in § 8, with each drum filling the upper 50 mm of a container.

In a global manner, two irradiation temperatures were chosen for the PYCASSO experiment in collaboration with our partners: 1000°C and 1200°C. Bearing in mind § 5.1.2, a maximum integrated fast fluence (E > 0.18 MeV) of $2 \cdot 10^{25}$ n/m^2 — or $2.183 \cdot 10^{25}$ n/m^2 (E > 0.10 MeV) equivalent to a maximum irradiation time of 123 EFPD – is still deemed acceptable.

The evaluation of the dose based on the neutron spectrum (cf. figure 10) [19] in the position G3-HFR and dpa cross sections of graphite and SiC (by assimilating PyC to graphite) results in an acquisition rate of 0.0126 $dpa_{graphite}$/EFPD and 0.00105 dpa_{SiC}/EFPD; respectively equivalent to 1.55 $dpa_{graphite}$ and 1.29 dpa_{SiC} for 123 EFPD.

11. CONCLUSION

The definition of this part of the PYCASSO irradiation experiment has been practically finalised, with the main objective being to acquire knowledge on densification kinetics in the pyrocarbon layers of fuel particles produced in current fuel fabrication processes

On the grounds on microstructural and statistical representativeness, the spherical geometry was chosen in preference to all other geometries.

It has been possible to establish the theory, methods and procedures used to determine the entities $\eta_{//}$ and $\eta_{\perp}$ inherent to practically unrestrained conditions in pyrocarbon layers based on the irradiation of spherical fuel particles with inert kernels.

In order to represent standard fuel as much as possible while corresponding to hypotheses behind the theory related to data processing, two fuel particle geometries with inert kernels were chosen (kernel diameters of 500 µm and 2000 µm).

The different types of fuel particles to be irradiated have been identified (arrangement of the different layers); however, the number of each fuel particle type remains to be specified taking into account the amount of available space and statistical aspects.

A preliminary design of the experimental device (drum) has been recommended.

Two particle operating temperatures have been chosen: 1000°C and 1200°C. The risk of incompatibility with the theory in question and thus PyC-buffer interactions (problem of relative densification) limits irradiation to a maximum integrated fast fluence (E > 0.18 MeV) of $2 \cdot 10^{25}$ n/m^2, which corresponds to 123 EFPD.

The possible temperature-fluence couples still need to be specified for the different levels of the HFR rig housing the drums.

The nature of the inert kernel remains to be established, even if corundum (Al_2O_3) looks promising.

The manufacturability of particles, particularly large-diameter particles, must be validated.

The provisional schedule is as follows:

- Sample specifications: October-December 2006,
- Feasibility-development: January-March 2007,
- Manufacturing: April-June 2007,
- Controls: July-September 2007,
- Delivery: 4th trimester 2007.

REFERENCES

[1] J.C. Bokros – 1965
Absorption Factors for a Modified Bacon Preferred-Orientation Technique
Carbon **3** : 167-174

[2] J.C. Bokros and R.J. Price – 1966
Radiation-Induced Dimensional Changes in Pyrolytic Carbons Deposited in a Fluidized Bed
Carbon **4** : 441-454

[3] J.L. Kaae – 1975
Irradiation-Induced Microstructural Changes in Isotropic Pyrolytic Carbons
Journal of Nuclear Materials **57** : 82-92

[4] J.L. Kaae – 1977
The Mechanical Behavior of BISO-Coated Fuel Particles During Irradiation.
Part I: Analysis of Stresses and Strains Generated in the Coating of a BISO Fuel Particle During Irradiation
Nuclear Technology **35 (2)** : 359-367

[5] J.L. Kaae – 1970
On Irradiation-Induced Creep of Pyrolytic Carbon in a General State of Stress
Journal of Nuclear Materials **34** : 206-208

[6] J.L. Kaae *et al.* – 1977
The Mechanical Behavior of BISO-Coated Fuel Particles During Irradiation.
Part II: Prediction of BISO Particle Behavior During Irradiation with a Stress-Analysis Model
Nuclear Technology **35 (2)** : 368-378

[7] K.S.B. Rose and R.H. Keep – 1975
A New Technique for Measuring the Dimensional Changes of Pyrocarbon
Journal of Nuclear Materials **57** : 353-355

[8] J.L. Kaae and J.C. Bokros – 1971
Irradiation-Induced Dimensional Changes and Creep of Isotropic Carbon
Carbon **9** : 111-122

[9] C.R. Kennedy – 1965
Second. Conf. Indust. Carbon and Graphite - London

[10] J.L. Kaae, S.A. Sterling and L. Yang – 1977
Improvements in the Performance of Nuclear Fuel Particles Offered by Silicon-Alloyed Carbon Coatings.
Nuclear Technology **35 (2)** : 536-547

[11] M. Phélip et G. Degenève – 2006
IAEA CRP6 Coated Particle Fuel Performance Benchmark–Normal Operation–ATLAS results
Note Technique SESC/LC2I 05-020 indice 0

[12] J.M. Escleine – 2003
Matériaux Inertes de Confinement pour Systèmes RCG-R et RCG-T
Réflexions sur les Orientations Techniques
Note Technique SESC/LIAC 03-018 indice 0

[13] E.A.C. Neeft *et al.* – 1999
Neutron Irradiation of Polycrystalline Yttrium Aluminate Garnet, Magnesium Aluminate Spinel and α-aluminia
Journal of Nuclear Materials **274** : 78-83

[14] M. Pelletier *et al.* – 2003
HTR-Project: Selection of Properties and Models For the Coated Particle – PyC and SiC
Note Technique SESC/LSC 03-0218 Indice 0

[15] K. Bongartz *et al* (H.A. Schulze Ed.) – 1974
Methods for the Characterization of Pyrolytic Deposited Carbon
Characterization Procedures Applied in the Institute für Reaktorwerkstoffe
Jül – 1078 – RW GERHTR - 134

[16] C. Rado et B. Deschamps – 2006
Compatibilité de UC et SiC avec Mo, Re et W
Note Technique DTEC/STCF/2006/12

[17] Y. Isobe *et al.* – 1989
Chemical Vapour Deposition of Rhenium on Graphite
Journal of the Less-Common Metals **152** : 177-184

[18] Y. Isobe *et al.* – 1989
Chemically Vapour-Deposited Mo/Re Double-Layer Coating
on Graphite at Elevated Temperatures
Journal of the Less-Common Metals **152** : 239-250

[19] H.L. Heinisch *et al.* – 2004
Displacement Damage in Silicon Carbide Irradiated in Fission Reactors
Journal of Nuclear Materials **327** : 175-181

FIGURES

FIGURE 1: COMPARISON WITH ATLAS – 0/0 MPA 45

FIGURE 2: COMPARISON WITH ATLAS – 0.1/0.1 MPA 46

FIGURE 3: COMPARISON WITH ATLAS – 0.072/1 MPA 47

FIGURE 4: CHANGE IN $\Delta b/b$ AND $\Delta e/e$ FOR DIFFERENT PRESSURE COUPLES – X = 0.9130 48

FIGURE 5: CHANGE IN $\Delta b/b$ AND $\Delta e/e$ FOR DIFFERENT PRESSURE COUPLES – X = 0.9794 49

FIGURE 6: INFLUENCE OF X ON THE INTENSITY OF SELF-GENERATED STRESSES (0/0 BAR) 50

FIGURE 7: CHANGES IN $\Delta(\Delta b/b)$ AND $\Delta(\Delta a/a)$ 51

FIGURE 8: BUFFER SHRINKAGE *VERSUS* OPYC – 500/170 µm 52

FIGURE 9: BUFFER SHRINKAGE *VERSUS* OPYC – 2000/400 µm 53

FIGURE 10: RELATIVE DISTRIBUTION OF NEUTRON ENERGIES IN G3-HFR POSITION 54

FIGURE 11: VARIATION IN $\delta\eta/|\eta|$ *VERSUS* FLUENCE - δb = 0.5 µm - δd = 0.0001 55

FIGURE 1: COMPARISON WITH ATLAS – 0/0 MPA

(A)

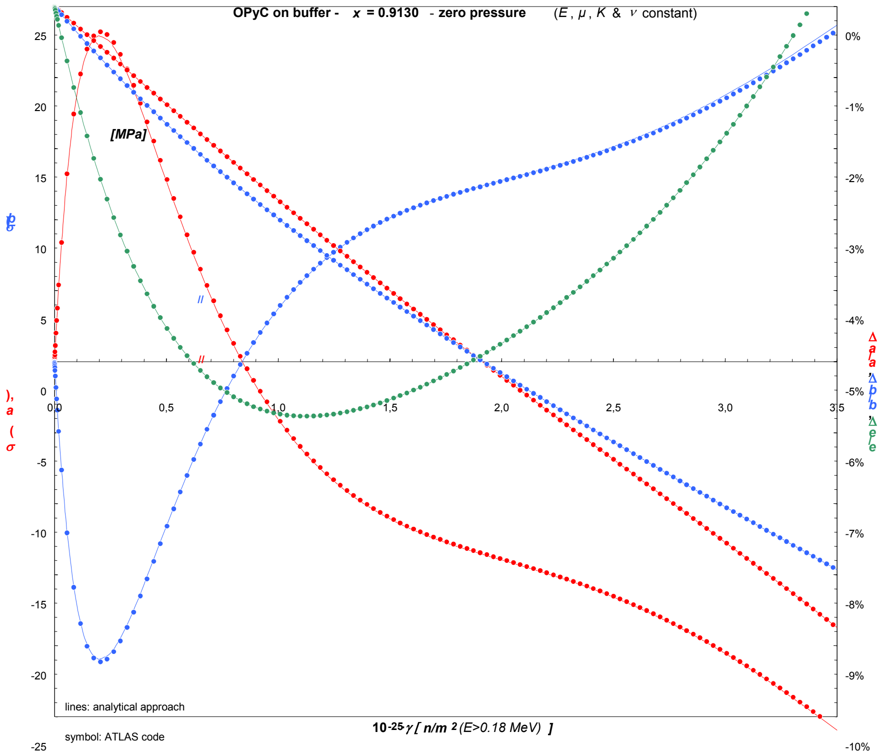

(B)

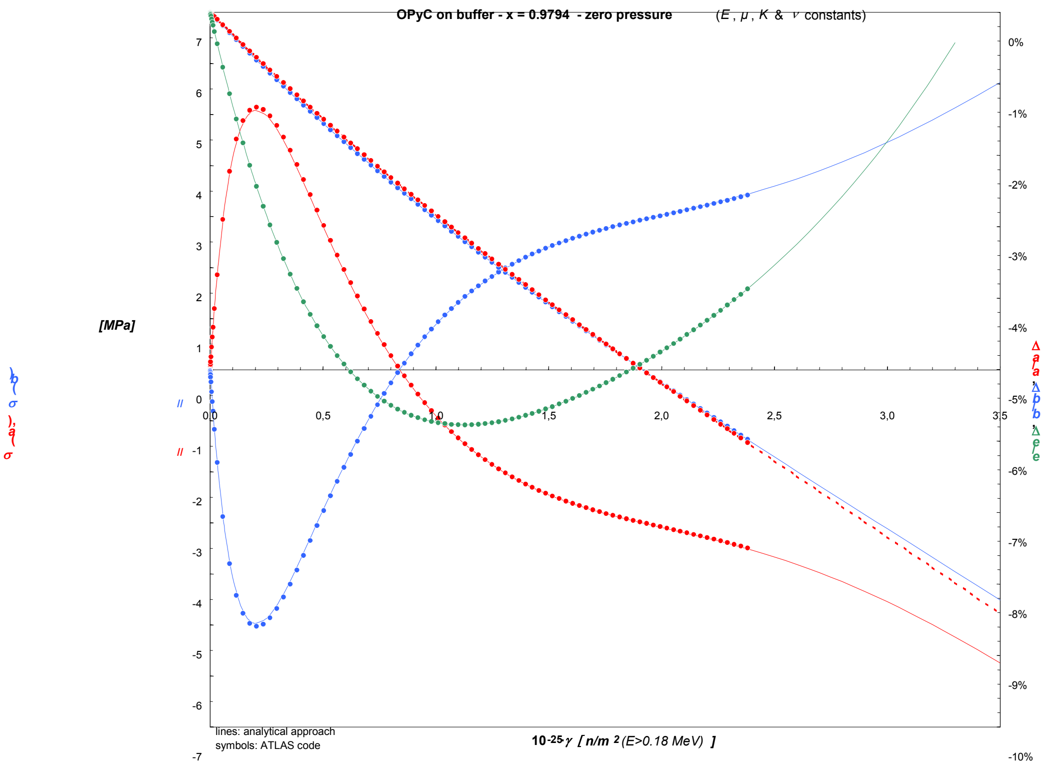

FIGURE 2: COMPARISON WITH ATLAS – 0.1/0.1 MPA

(A)

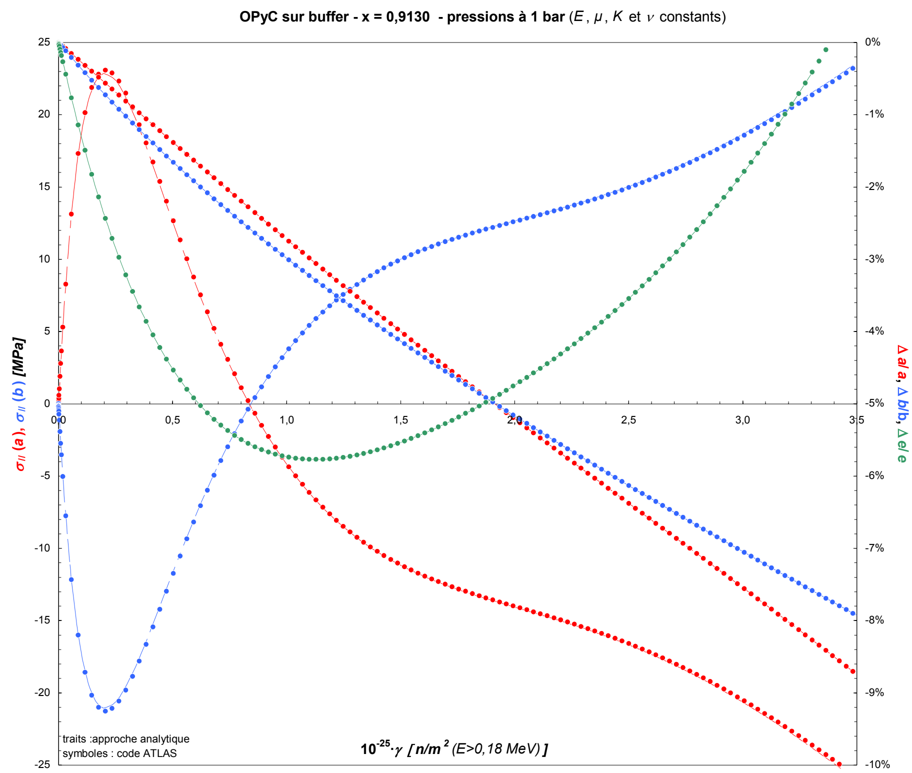

(B)

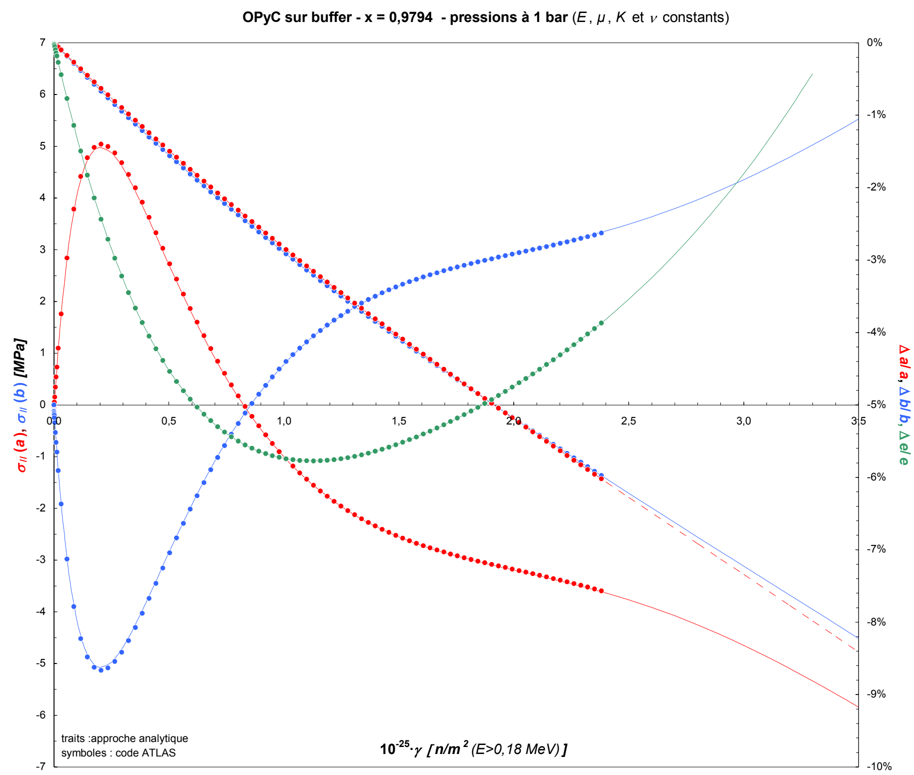

FIGURE 3: COMPARISON WITH ATLAS – 0.072/1 MPA

(A)

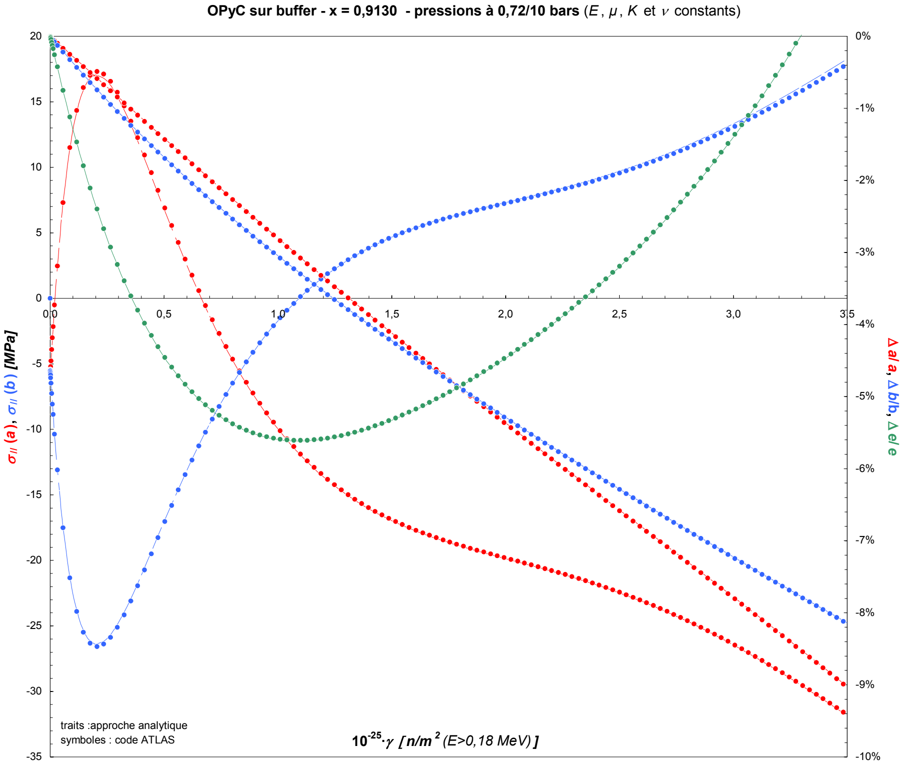

(B)

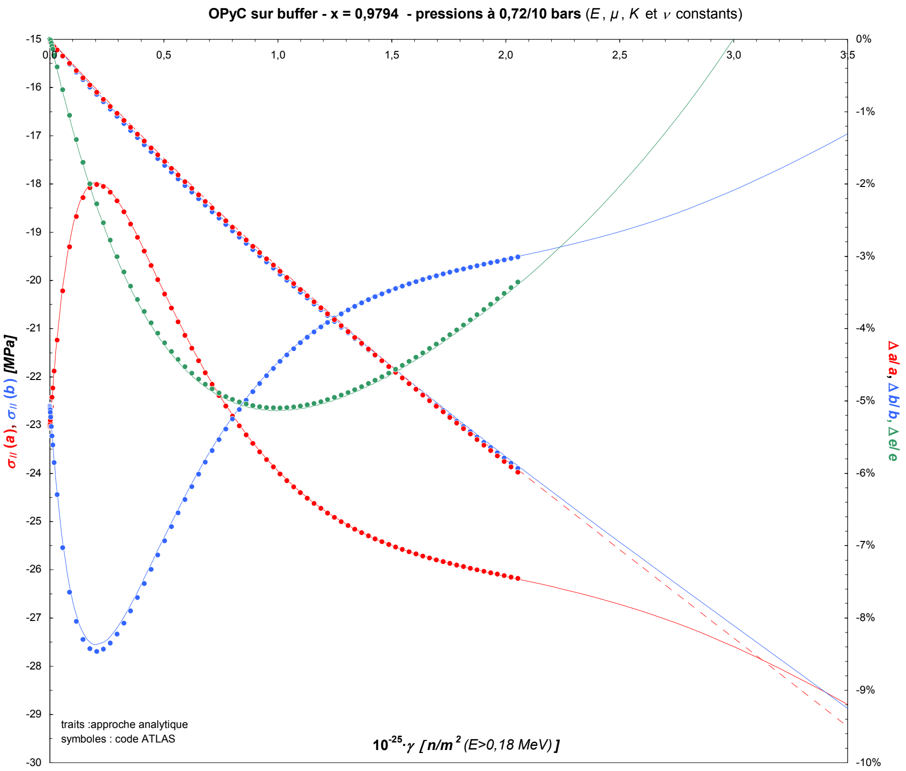

FIGURE 4: CHANGE IN $\Delta b/b$ AND $\Delta e/e$ FOR DIFFERENT PRESSURE COUPLES – x = 0.9130

(A)

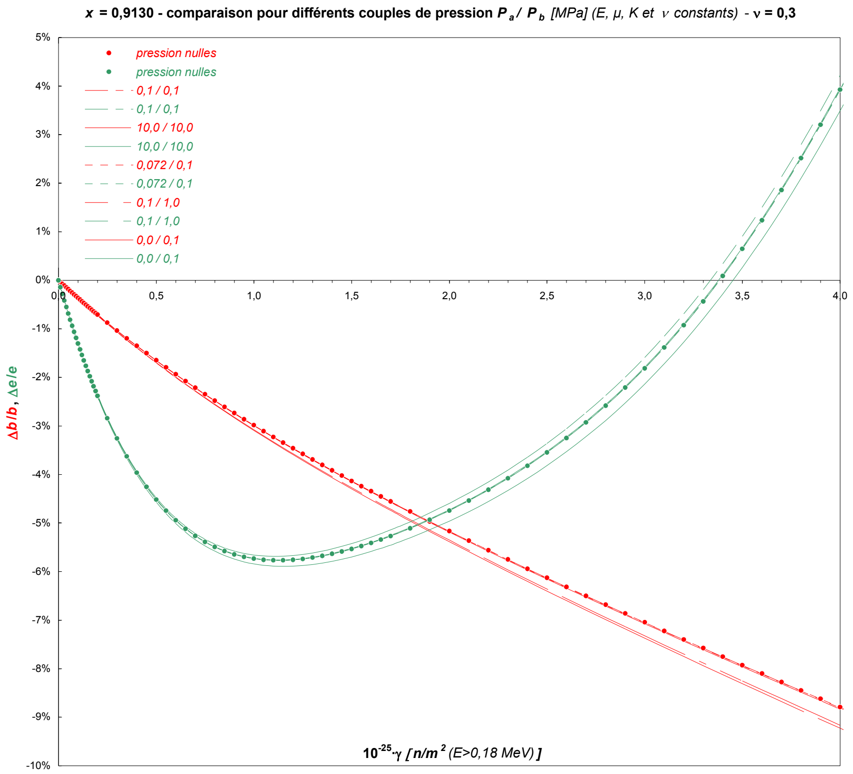

(B)

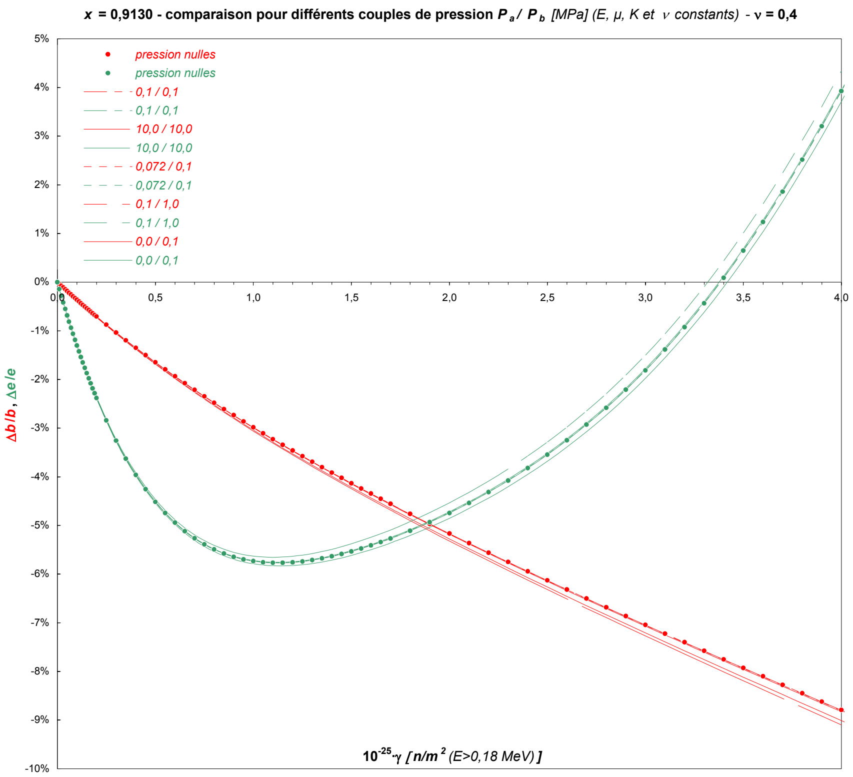

FIGURE 5: CHANGE IN $\Delta b/b$ AND $\Delta e/e$ FOR DIFFERENT PRESSURE COUPLES – x = 0.9794

(A)

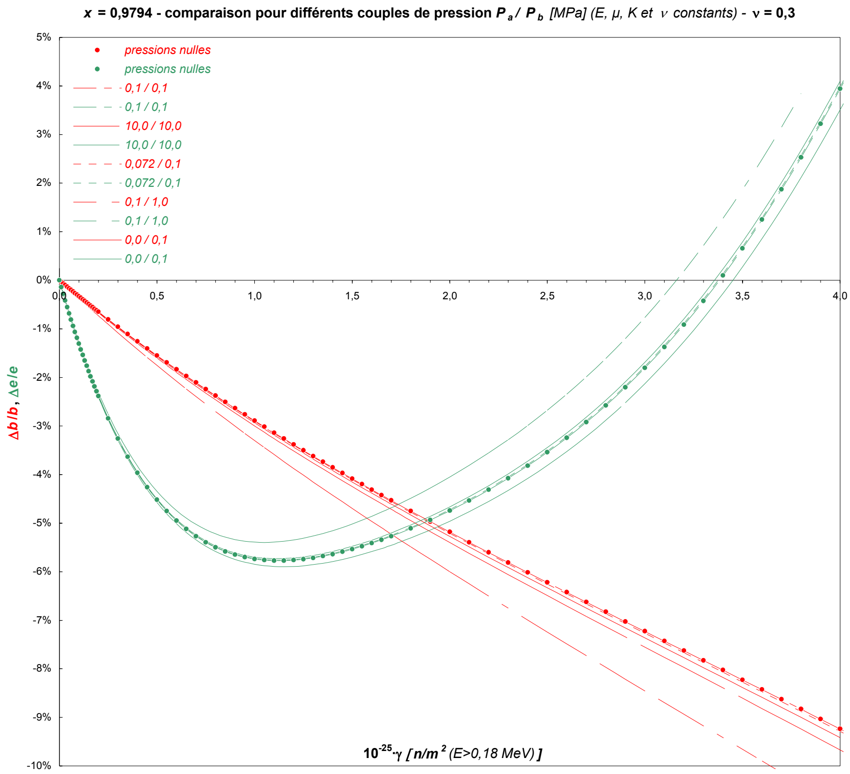

(B)

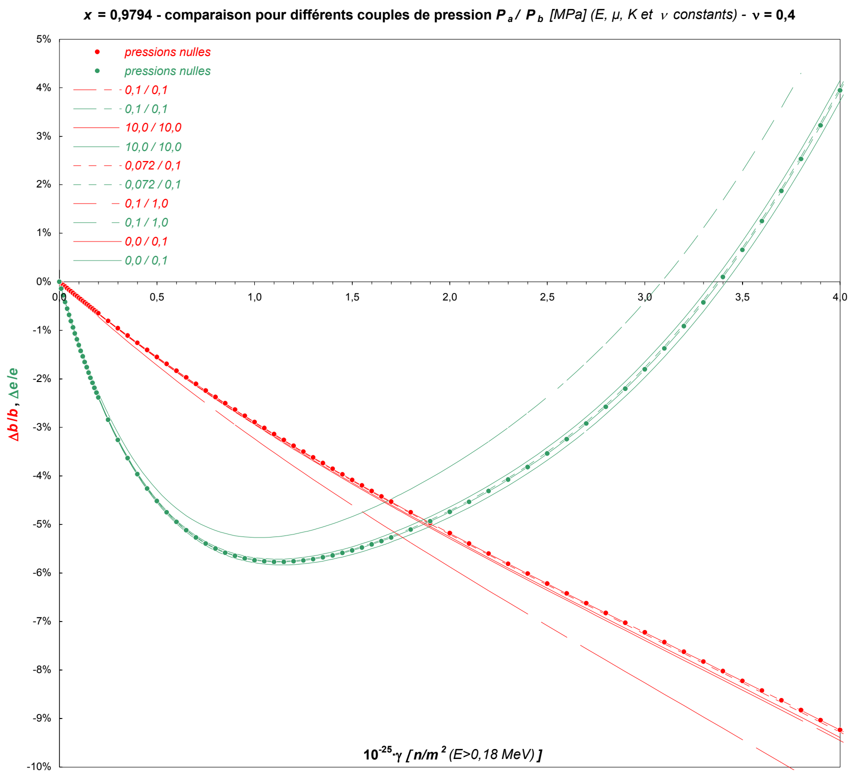

FIGURE 6: INFLUENCE OF *X* ON THE INTENSITY OF SELF-GENERATED STRESSES (0/0 BAR)

(A)

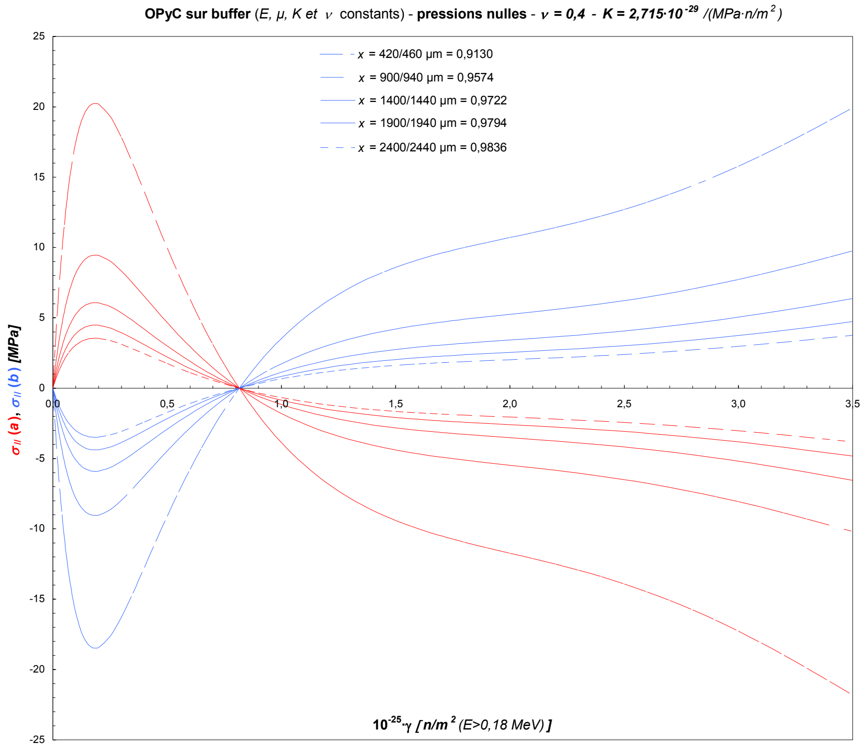

(B)

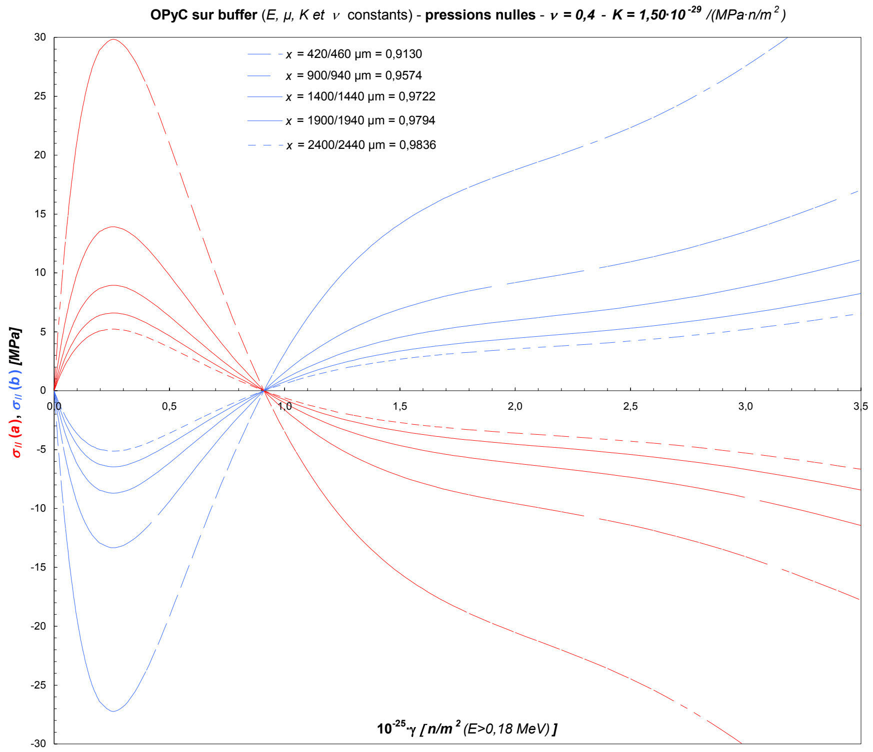

FIGURE 7: CHANGES IN $\Delta(\Delta b/b)$ AND $\Delta(\Delta a/a)$

(A)

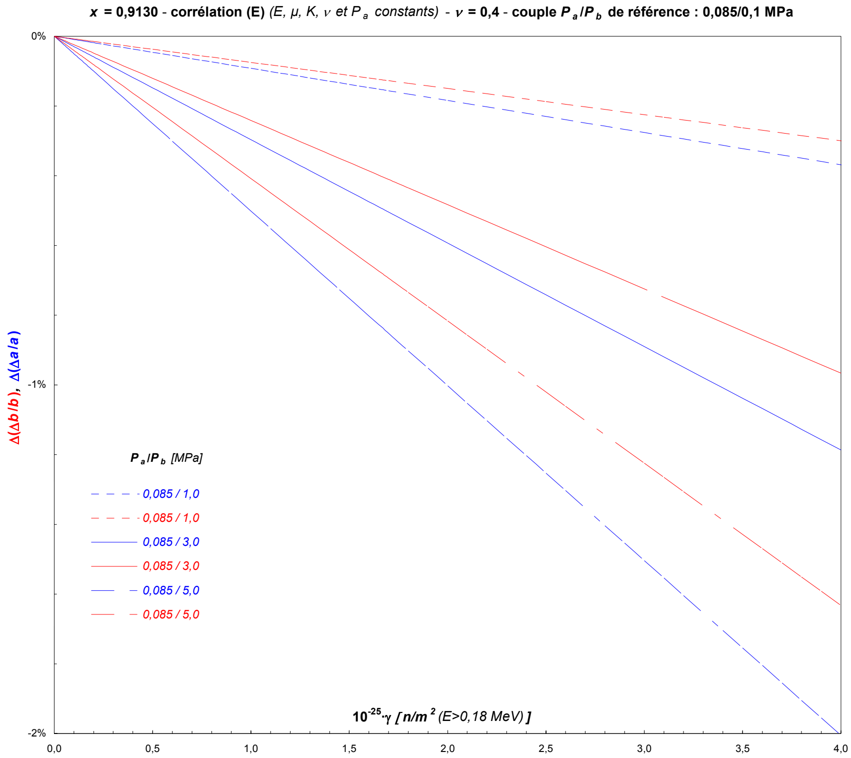

(B)

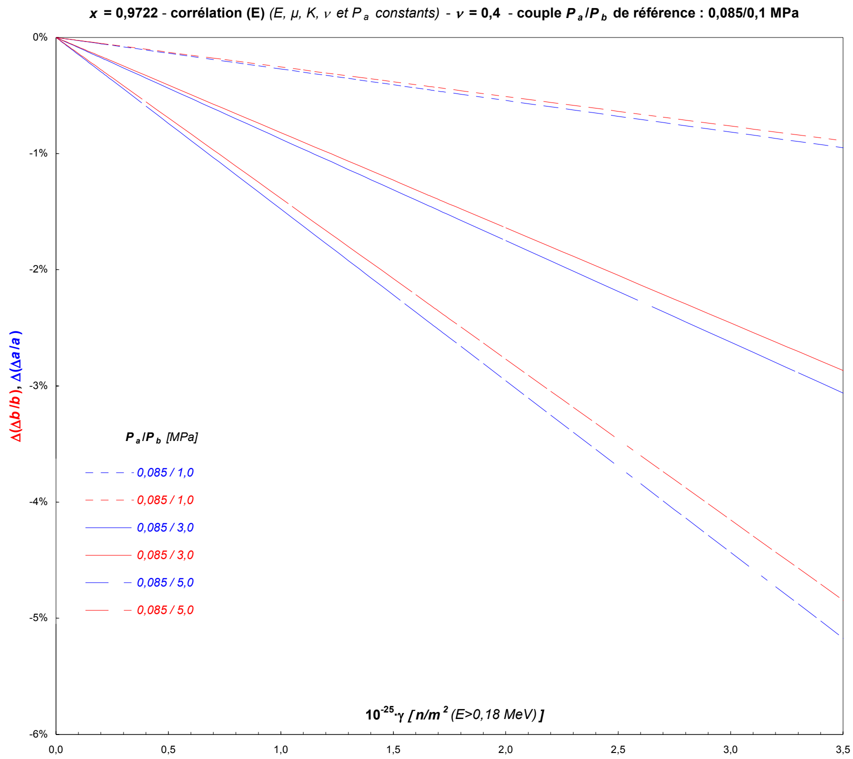

FIGURE 8: BUFFER SHRINKAGE *VERSUS* OPYC – 500/170 µm

(A)

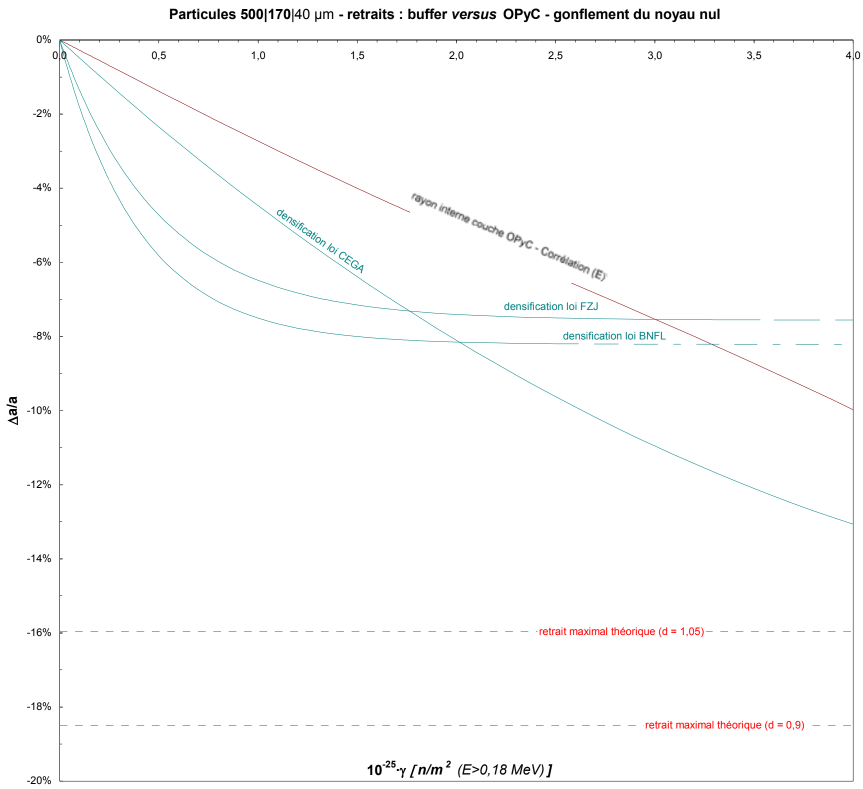

(B)

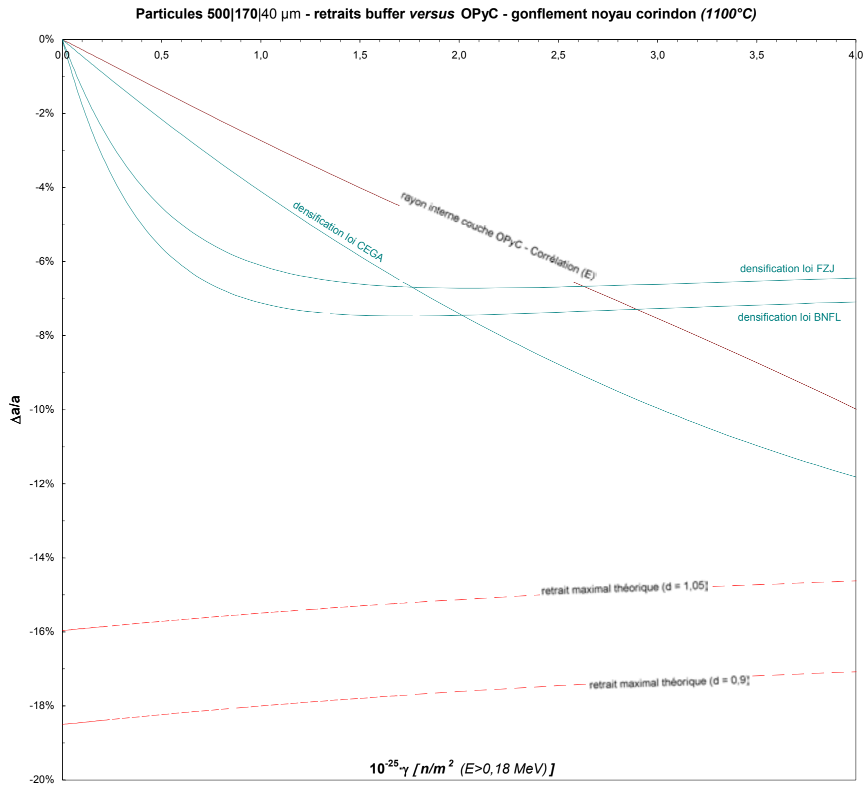

FIGURE 9: BUFFER SHRINKAGE *VERSUS* OPYC – 2000/400 µm

(A)

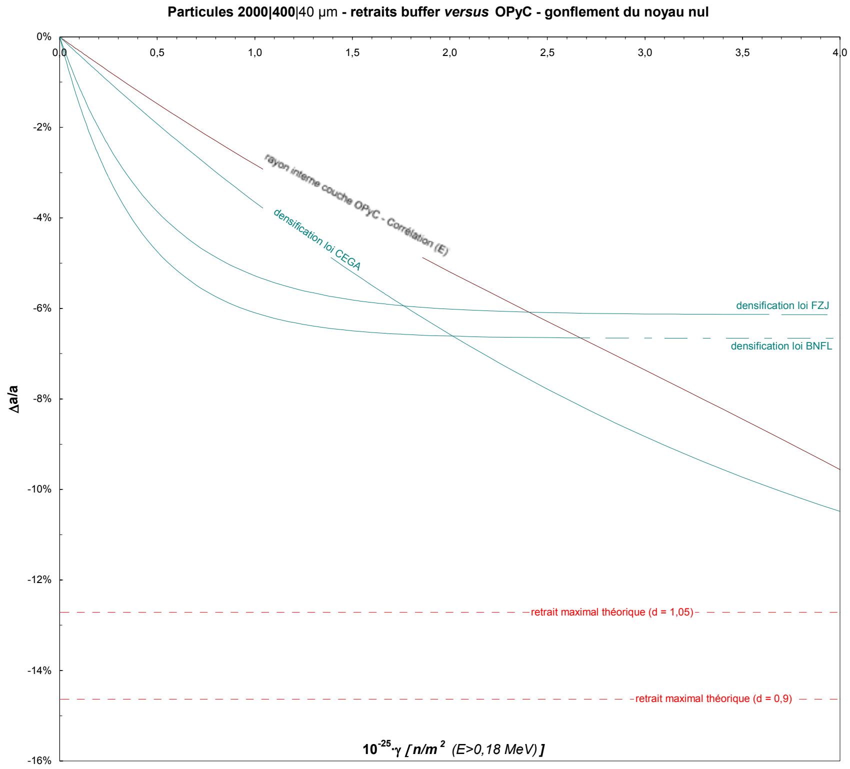

(B)

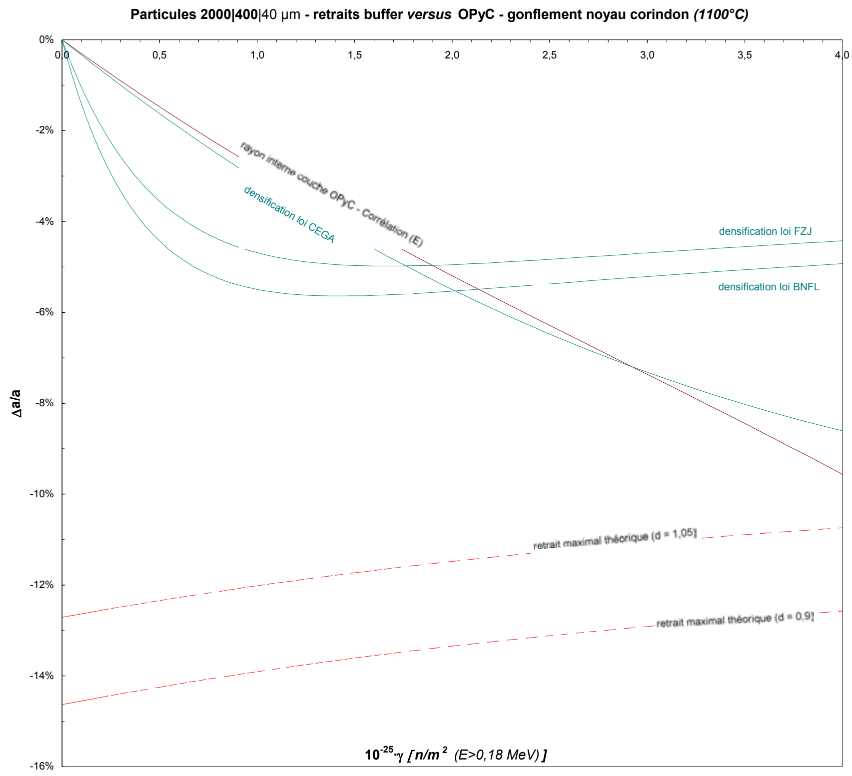

FIGURE 10: RELATIVE DISTRIBUTION OF NEUTRON ENERGIES IN G3-HFR POSITION

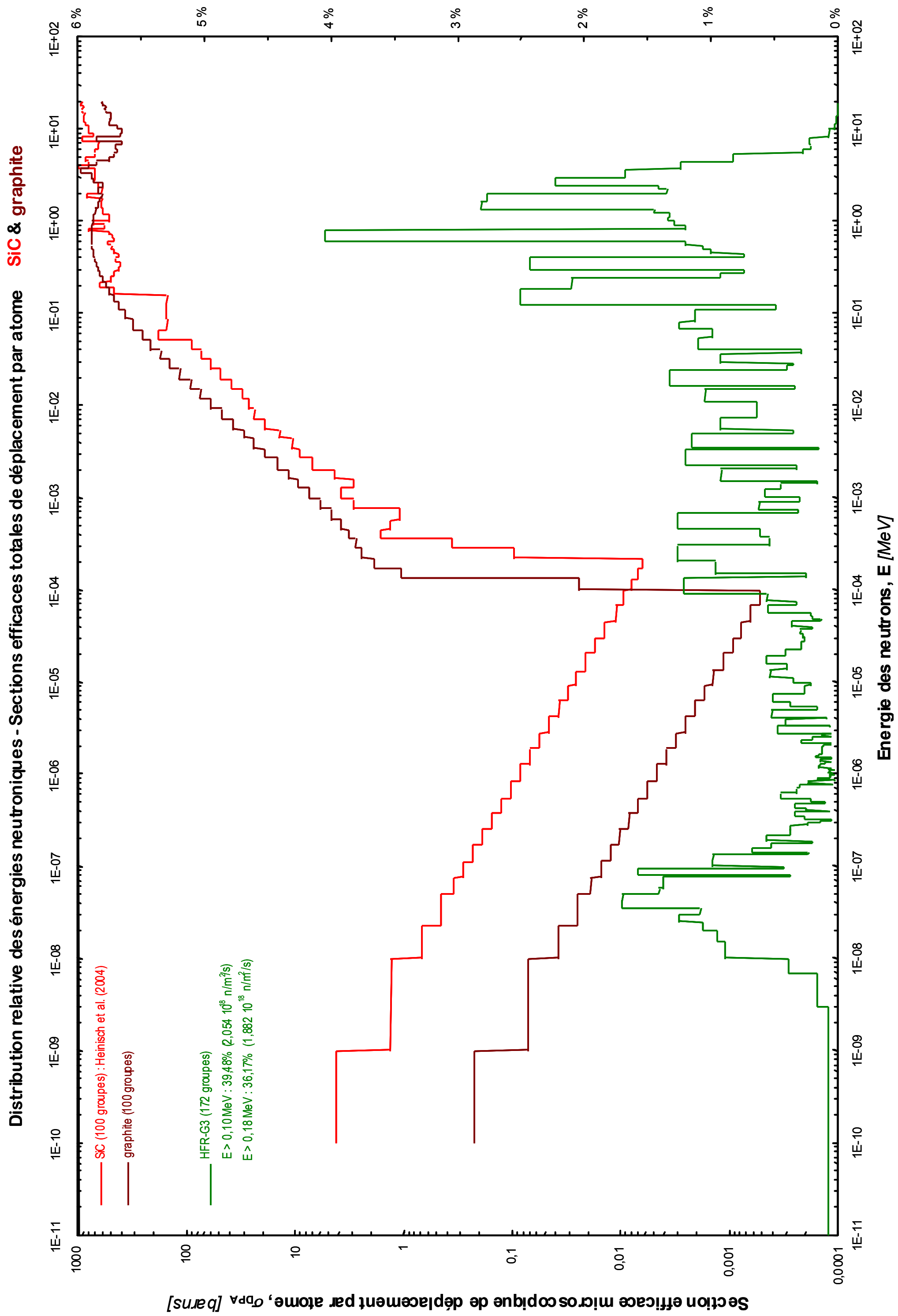

FIGURE 11: VARIATION IN $\delta\eta/|\eta|$ *VERSUS* FLUENCE - δb = 0.5 µm - δd = 0.0001